

PAPER

# Loschmidt echo and Poincaré recurrences of entanglement

To cite this article: Leonardo Ermann *et al* 2022 *J. Phys. A: Math. Theor.* **55** 234004

View the [article online](#) for updates and enhancements.

## You may also like

- [Quantitative recurrence for free semigroup actions](#)  
Maria Carvalho, Fagner B Rodrigues and Paulo Varandas
- [Poincaré recurrence theory and its applications to nonlinear physics](#)  
V S Anishchenko and S V Astakhov
- [Hitting time statistics for observations of dynamical systems](#)  
Jérôme Rousseau



**IOP | ebooks™**

Bringing together innovative digital publishing with leading authors from the global scientific community.

Start exploring the collection—download the first chapter of every title for free.

# Loschmidt echo and Poincaré recurrences of entanglement

Leonardo Ermann<sup>1,2</sup>, Klaus M Frahm<sup>3</sup>  
and Dima L Shepelyansky<sup>3,\*</sup> 

<sup>1</sup> Departamento de Física Teórica, GIyA, Comisión Nacional de Energía Atómica, Av. del Libertador 8250, 1429 Buenos Aires, Argentina

<sup>2</sup> Consejo Nacional de Investigaciones Científicas y Técnicas (CONICET), C1425FQB, Buenos Aires, Argentina

<sup>3</sup> Laboratoire de Physique Théorique du CNRS, Université de Toulouse, UPS, 31062 Toulouse, France

E-mail: [dima@irsamc.ups-tlse.fr](mailto:dima@irsamc.ups-tlse.fr)

Received 7 January 2022, revised 7 April 2022

Accepted for publication 27 April 2022

Published 16 May 2022



CrossMark

## Abstract

We study numerically the properties of entanglement of two interacting, or non-interacting, particles evolving in a regime of quantum chaos in the quantum Chirikov standard map. Such pairs can be viewed as interacting, or non-interacting, Einstein–Podolsky–Rosen pairs in a regime of quantum chaos. The analysis is done with such tools as the Loschmidt echo of entanglement and the Poincaré recurrences of entanglement in presence of absorption. The obtained results show unusual features of the entropy of entanglement and the spectrum of Schmidt decomposition with their dependence on interactions at different quantum chaos regimes.

Keywords: Loschmidt, echo, Poincaré, recurrences, entanglements, quantum chaos, entanglement

 Supplementary material for this article is available [online](#)

(Some figures may appear in colour only in the online journal)

## 1. Introduction

The ancient dispute between Loschmidt and Boltzmann about emergence of statistical laws from time reversible dynamical equations [1–3] (see also [4]) found its modern resolution

\*Author to whom any correspondence should be addressed.

on the basis of phenomenon of dynamical chaos with its exponential instability of trajectories which breaks the time reversal in presence of exponentially small errors [5–8]. In quantum mechanics this exponential instability of chaos has been shown to exist only on a logarithmically short Ehrenfest time scale [9–12]:

$$t_E \sim (\ln q)/h = \ln(I/\hbar)/h, \quad (1)$$

where  $q = I/\hbar$  is a typical quantum number,  $I$  is a corresponding classical action,  $\hbar$  is the Planck constant and  $h \geq \Lambda$  is the Kolmogorov–Sinai entropy [5–8] which is larger or equal to the Lyapunov exponent of a dynamical chaotic trajectory. This time  $t_E$  is so short due to an exponentially rapid spreading of minimal coherent wave packet so that after this time the Ehrenfest theorem [13] loses its validity.

Various properties of quantum chaos of one-particle quantum evolution, which is chaotic in the classical limit, are described and reviewed in [9, 11, 14, 15]. While the classical chaotic dynamics breaks time reversal due to the exponential growth of errors, in [16] it was shown that in the regime of quantum chaos the time reversal remains stable even if the numerical simulations are done on the same computer for classical and quantum evolution. This result was obtained for the Chirikov standard map which describes the generic features of chaotic dynamics with divided phase space [7, 8, 17]. The studies of effects of Hamiltonian perturbations acting on the quantum evolution during the return path of time reversal have been extended in [18] and the decoherence effects for this Loschmidt echo have been analyzed in [19] with links to the Lyapunov exponent. Various interesting properties of Loschmidt echo have been studied by different groups being described in [20–23]. In the context of quantum computing the properties of fidelity and Loschmidt echo for time reversal were reported in [24, 25]. The time reversal of atomic Bose–Einstein condensate in the regime of quantum chaos of the Chirikov standard map was experimentally realized by the Hoogerland group [26], following the theoretical proposal [27].

The above studies of the time reversal and Loschmidt echo are done for one particle quantum evolution. However, it is also interesting to analyze the properties of entanglement in systems of quantum chaos. Indeed, the fundamental work of Einstein–Podolsky–Rosen (EPR) [28] about a distant entanglement [29] of a pair of noninteracting distinguishable particles is now at the foundations of quantum information and communications [30–32].

Recently, the properties of chaotic EPR pairs without interactions, the effects of time reversal and measurements were analyzed for the quantum Chirikov map in [33]. Here, the Schmidt decomposition of the EPR wavefunction [34] (see also [35]) is found to be especially useful. Without interactions the entropy of entanglement  $S$  of the EPR pair [30, 31] is preserved during a quantum evolution. Thus it is interesting to study how this quantity and Loschmidt echo  $M(t)$  are affected by interactions between particles. With this aim we present here the analysis of these quantities for chaotic EPR pairs with interactions in the quantum Chirikov standard map. This model was already investigated in [36, 37] in the context of interaction effects on the dynamical localization but the entropy of entanglement was not studied there.

In addition, we also study how the entropy of entanglement  $S$  in this model is affected by the absorption of one or two particles. In a certain sense the absorption can be considered as some kind of measurement and it is interesting to understand its influence on EPR characteristics. We note that in the case of quantum evolution of one particle the effects of absorption have been studied in this system in [38–43]. The probability that a particle remains inside the system can be considered as a quantum version of Poincaré recurrences [44] which in the classical case of fully chaotic system decays exponentially with time while in the case of divided phase space with stability islands the decay is algebraic (see [45, 46] and references therein). Thus, in this

work we study the decay of Poincaré recurrences of entanglement for a chaotic EPR pair with and without interactions.

This paper is constructed as follows: the model is described in section 2, the Loschmidt echo of entanglement is studied in section 3, various cases of Poincaré recurrences of entanglement are analyzed in sections 4–6 and discussion of the results is given in section 7 (specific points are presented in the appendix A and additional data are given in supplementary material (<https://stacks.iop.org/JPA/55/234004/mmedia>) (SupMat)).

## 2. Model description

For one particle the classical dynamics is described by the Chirikov standard map [7]:

$$\bar{p} = p + k \sin x, \quad \bar{x} = x + T\bar{p}. \quad (2)$$

Here  $x$  represents a cyclic variable  $0 \leq x < 2\pi$  for the case of the kicked rotator,  $p$  is the particle momentum. The bars denote the new values of variables after one iteration of this symplectic map. The dynamics depends on a single chaos parameter  $K = kT$  with a transition from integrability to unlimited chaotic diffusion in momentum for  $K > K_c = 0.9715 \dots$  [7, 8]. The system dynamics is reversible in time, e.g. by inverting all velocities in a middle of free rotation between two kicks [16]. This map captures the generic properties of chaos in systems with integrable islands surrounded by chaotic components, its applications to various physical systems are summarized in [17].

The dynamics in a chaotic component has a positive Kolmogorov–Sinai entropy  $h$  which characterizes the exponential divergence of nearby trajectories. For  $K > 4$  we have  $h \approx \ln(K/2)$  [7]. For  $K > K_c$  there is an unlimited diffusive momentum growth with time  $t$ , measured in number of map iterations:  $\langle (\Delta p)^2 \rangle = 2Dt$  with a diffusion coefficient  $D \approx k^2/4$  (see more details in [7, 47]).

The quantum state  $|\psi\rangle$  propagation over a period is given by a unitary operator (here still for one particle)  $U_{\text{KR}}^{(1)}$  [9, 11]:

$$|\bar{\psi}\rangle = U_{\text{KR}}^{(1)}|\psi\rangle = e^{-iT\hat{p}^2/2} e^{-ik \cos \hat{x}}|\psi\rangle. \quad (3)$$

Here the momentum  $p$  is measured in recoil units of the optical lattice with  $\hat{p} = -i\partial/\partial x$ . Hence,  $T = \hbar$  plays the role of an effective dimensionless Planck constant and the classical limit corresponds to  $T = \hbar \rightarrow 0$ ,  $k \rightarrow \infty$ ,  $K = kT = \text{const}$ . Here we consider the case of a kicked rotator with a wave function (in position representation)  $\psi(x) = \langle x|\psi\rangle$  being periodic on a circle  $\psi(x + 2\pi) = \psi(x)$ . In this case the free rotation corresponds (in momentum representation) to the phase shift  $\bar{\psi}_n = \exp(-iTn^2/2)\psi_n$  with  $\psi_n = \langle p|\psi\rangle$  being the wave function (in momentum representation) at  $p = n$ . The effects of quantum interference lead to dynamical localization of chaotic diffusion on a time scale  $t_D \approx D/\hbar^2 \gg t_E$  and an exponential localization of quasienergy eigenstates with a localization length  $\ell = D/(\hbar^2) \approx k^2/4$  [11, 47–49]. This dynamical localization is similar to the Anderson localization of electrons in a disordered solid [50] and it has been observed in experiments with cold atoms in kicked optical lattices in [51, 52]. The time reversal of atomic waves in this system has been realized in [26] following the theoretical proposal [27].

For two noninteracting or interacting particles the evolution operator  $U_{\text{KR}}$  is given by:

$$U_{\text{KR}} = \exp(-iT(\hat{p}_1^2 + \hat{p}_2^2)/4 + i\hat{U}/2) \times \quad (4)$$

$$\exp(-ik \cos \hat{\theta}_1 - ik \cos \hat{\theta}_2) \times \quad (5)$$

$$\exp(-iT(\hat{p}_1^2 + \hat{p}_2^2)/4 + i\hat{U}/2). \quad (6)$$

Here  $\hat{U}$  is the interaction operator which is diagonal in momentum representation with eigenvalues being either  $U$  for  $p_1 = p_2$ ,  $U/2$  for  $0 < |p_1 - p_2| \leq U_r$  or 0 for other cases with  $|p_1 - p_2| > U_r$  with  $p_{1,2} = n_{1,2}$  being momentum of first and second particle. Here  $U$  is the interaction strength parameter and  $U_r$  is the interaction range (chosen as  $U_r = 0$  or  $U_r = 1$  in this work). At  $U_r = 0$  we have the case of Hubbard on-site interaction which was first studied in [36, 37] for the kicked rotator. The difference  $|p_1 - p_2|$  is computed with respect to the periodic boundary conditions, i.e.,  $|p_1 - p_2| = 1$  if for example  $p_1 = N/2 - 1$  and  $p_2 = -N/2$  and similarly for other cases;  $\hat{\theta}_j$  represents the usual phase operator of particle  $j$ . Here  $N$  gives the number of momentum states for each kicked rotator, for two of them there  $N^2$  momentum states.

We also mention that in (4)–(6), we use, in contrast to (3), the symmetrized version of the map where a half free rotation is applied before and after the kick operator. This point is important to keep the time reversal symmetry and in particular for the studies in the next section.

Here we consider a short range interaction between two rotators in momentum space. This is very natural due to the analogy with disordered solid-state systems since for one rotator the chaotic diffusion and Anderson like localization [50] takes place in momentum space (the momentum space in the rotator plays the role of coordinate space in such solid-state systems, see references [36, 37, 47–49]).

### 3. Loschmidt echo of entanglement

In this section we consider the case of Hubbard on-site interaction of the quantum kicked rotator given by equation (4)–(6) with  $U_r = 0$  and  $U = 2$ . The other system parameter values are  $N = 2^{10} = 1024$ ,  $T = \hbar = \epsilon = 5/8$ , and  $K = 5$  such that  $k = K/\hbar = 8$ . As initial state we take a non-entangled state with  $p_1 = 0$ ,  $p_2 = 1$ :

$$|\psi(t=0)\rangle = |p_1 = 0\rangle \otimes |p_2 = 1\rangle. \quad (7)$$

The entropy of entanglement is given by (see e.g. [30]; see also the next section and appendix A.1 for additional details on the entropy computation and the numerical method for the quantum time evolution)

$$S(t) = -\text{Tr}[\rho_1 \log_2(\rho_1)], \quad (8)$$

where  $\rho_1$  is the reduced density matrix for the first particle obtained by a trace over the second particle.

In order to study the Loschmidt echo, we compute the time evolution forward in time with parameter values  $U_f$  and  $k_f$ :  $U_{\text{KR}}(U_f, k_f)$  till  $t = t_r$  where the time reversal takes place and then backward in time  $U_{\text{KR}}(U_b, k_b)$  till reaching  $t = 2t_r$ . We analyze the cases of  $U_f = U$ ,  $U_b = U_f + \Delta U$ ,  $k_b = k_f = k$ ; and  $U_f = U_b = U$ ,  $k_f = k$ ,  $k_b = k_f + \Delta k$ .

Figure 1 shows the time dependence of the entropy of entanglement (8) with  $t_r = 50$  and:  $U_f = U = 2$ ,  $U_b = U + \Delta U$  and  $k_b = k_f = k = 8$  with  $\Delta U = 0, 0.3, 0.5$  in left panel; and  $U_f = U_b = 2$ ,  $k_f = k = 8$  and  $k_b = k + \Delta k$  with  $\Delta k = 0, 0.03, 0.05$ . We have verified that a further increase of  $N$  to values of  $10^{11} = 2048$  and  $10^{12} = 4096$  provide identical results up to numerical round-off errors. The results show that finite perturbations  $\Delta U$  or  $\Delta k$  break time reversal of entropy of entanglement  $S(2t_r)$ .

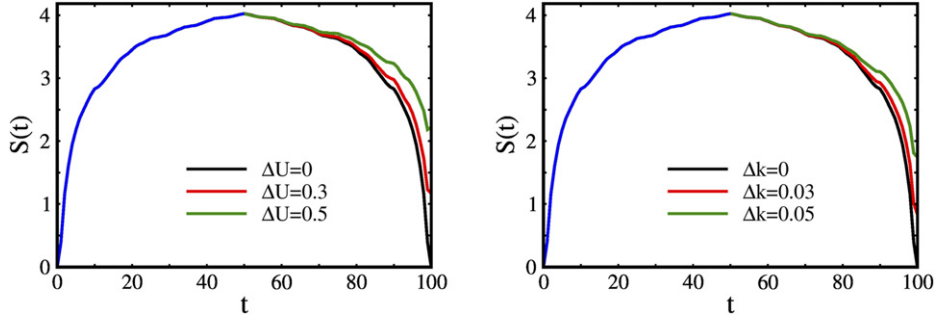


**Figure 1.** Time dependence of the entropy of entanglement  $S$  for the initial state  $|\psi(t=0)\rangle = |p_1=0\rangle \otimes |p_2=1\rangle$  with time evolution given by the quantum Chirikov standard map. The time reversal is performed after  $t_r = 50$  quantum map iterations. The blue curve in both panels show the forward time evolution  $0 \leq t \leq t_r$ , the black curves show the backward time evolution  $t_r \leq t \leq 2t_r = 100$  with the exact time reversal using  $T = 4\pi - \epsilon$ . (Left panel) Curves of other colors show the backward time evolution with perturbation  $U_b = U_f + \Delta U$  at  $\Delta U = 0.3$  (red curve) and  $\Delta U = 0.5$  (green curve). (Right panel) Curves of other colors show the backward time evolution with  $k_b = k_f + \Delta k$  at  $\Delta k = 0.03$  (red curve) and  $\Delta k = 0.05$  (green curve);  $U_f = U_b = U$ . The system parameters are:  $N = 1024$ ,  $T = \hbar = \epsilon = 5/8$ ,  $U = U_f = 2$ , and  $k = K/\hbar = 8$ .

The probability distributions in momentum of the first particle ( $p_1 = n_1$ )  $w(p_1, t) = \langle p_1 | \rho_1(t) | p_1 \rangle$ , taken at different moments in time, are presented in color in figure 2 for  $\Delta U = 0$  (left panel) and  $\Delta U = 0.5$  (right panel) with  $t_r = 50$  and the same other parameter values of figure 1. The color bar scale correspond to  $[w(p_1, t)/w_{\max}(t)]$  with  $w_{\max}(t) = \max_{p_1} w(p_1, t)$  being the density maximum at a given value of  $t$ . We see that the perturbation  $\Delta U$  is relatively weak and the global profile of density distribution  $w(p_1, t)$  is only weakly perturbed as compared to the case of exact time reversal. However, in the next figures we show that the echo characteristics are more sensitive to perturbations.

The entropy of entanglement of the initial state is obviously zero  $S(t=0) = 0$ , and when  $U_b = U_f$  and  $k_b = k_f$  the initial state is perfectly recovered for  $t = 2t_r$ . We also analyze the entropy of entanglement after  $2t_r$  steps given by  $G = S(2t_r)$  as a function of  $t_r$  at various perturbation values  $\Delta U = 0.1, 0.2, 0.3, 0.4, 0.5, 0.6$  with  $U_b = U_f + \Delta U$  and  $k_b = k_f = k = 8$ . The results are shown in figure 3. Left and right panels show the cases for  $U = 0$  and  $U = 2$  respectively. Initially  $G(t_r)$  grows linearly with time reversal  $t_r$  and it can be described as  $G(t_r) = S(2t_r) = \alpha t_r$ . At higher times the growth is saturated since both particles are localized in this system (see [36, 37]).

We also study the usual Loschmidt echo defined as (see e.g. [19]):

$$M(t_r) = |\langle \psi(t=0) | U_{\text{KR}}^\dagger(U_b, k_b)^{t_r} U_{\text{KR}}(U_f, k_f)^{t_r} | \psi(t=0) \rangle|^2, \quad (9)$$

where the initial state evolves  $t_r$  steps with forward parameter values  $U_f, k_f$  and then  $t_r$  steps with backward parameter values  $U_b, k_b$ . Figure 4 shows the Loschmidt echo as a function of time reversal  $t_r$  for the same parameters of figure 1 with  $U = 0$  and  $U = 2$  in left and right panels respectively where  $\Delta U = 0.1; 0.2; 0.3; 0.4; 0.5; 0.6$  and  $k_b = k_f = 8$ . At short times the decrease of the echo  $M(t_r)$  can be described as the exponential decay  $M(t_r) = \exp(-\Gamma t_r)$ .

We have fitted curves of figure 3 in the interval  $t_r \in [0, 10/\Delta U]$  by the linear fit  $G(t_r) = \alpha t_r$ . The obtained values of  $\alpha$  for  $U = 0, U = 2$ , and  $\Delta U = 0.1, 0.2, 0.3, 0.4, 0.5, 0.6$  are shown in

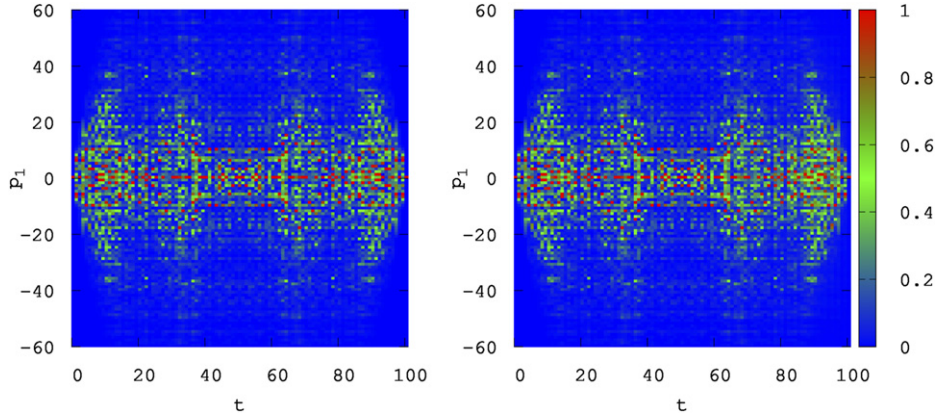


**Figure 2.** Time evolution of probability of the first particle  $w(p_1, t)$  (color density plot) for  $U = 0$ ,  $t_r = 50$ ,  $N = 1024$ ,  $\hbar_{\text{eff}} = \epsilon = 5/8$ ,  $k = K_{\text{eff}}/\hbar_{\text{eff}} = 8$  and  $-60 \leq p_1 \leq 60$  (y-axis),  $0 \leq t \leq 100$  (x-axis). The color bar gives values of  $[w(p_1, t)/w_{\text{max}}(t)]$  with  $w_{\text{max}}(t) = \max_{p_1} w(p_1, t)$  being the density maximum at a given value of  $t$ . (Left panel) Shows the case of  $\Delta U = 0$  (corresponding to the black curve of figure 1 left panel); (right panel) represents the case of  $\Delta U = 0.5$  (corresponding to the green curve of figure 1 left panel).

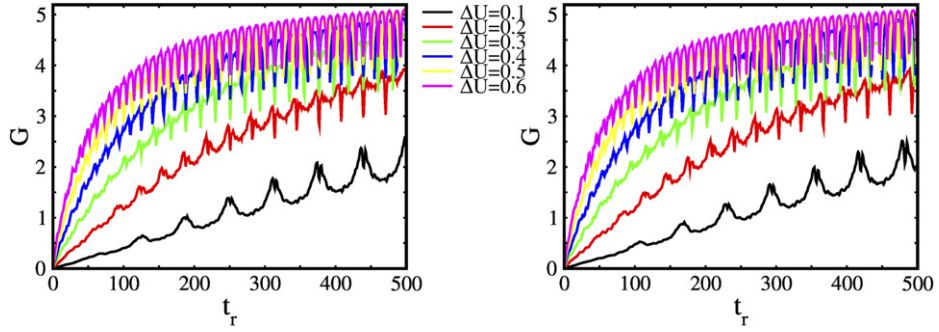


**Figure 3.** Loschmidt echo of entropy of entanglement at time  $2t_r$  ( $G = S(2t_r)$ ) as a function of  $t_r$ . (Left panel and right panel) Show the cases of  $U = 0$  and  $U = 2$  respectively with  $\Delta U = 0.1; 0.2; 0.3; 0.4; 0.5; 0.6$ . Other parameter values are the same as in figure 1.

the right panel of figure 5. Since the Loschmidt echo decays exponentially with time reversal  $t_r$  for short times, we have fitted the curves of figure 4 in the interval  $t_r \in [0, 10/\Delta U]$  with  $M(t_r) = \exp(-\Gamma t_r)$ . The obtained values  $\Gamma$  for  $U = 0$  and  $U = 2$ , and  $\Delta U = 0.1, 0.2, 0.3, 0.4, 0.5, 0.6$  are shown in the left panel of figure 5.

The results presented in figure 5 show that the dependence of  $\Gamma$  and  $\alpha$  of perturbation  $\Delta U$  is well described by the quadratic growth:  $\Gamma = A(\Delta U)^2$  and  $\alpha = B(\Delta U)^2$  with the fit values  $A = 0.030 \pm 0.001$  (for  $U = 0$ ),  $A = 0.031 \pm 0.001$  (for  $U = 2$ );  $B = 0.169 \pm 0.002$  (for  $U = 0$ ),  $B = 0.172 \pm 0.002$  (for  $U = 2$ ). Such a dependence appears naturally from the Fermi golden rule and is well known for the usual Loschmidt echo in the case of a small parameter perturbation (see e.g. [20–22]). For the Loschmidt echo of entanglement  $G(t_r)$  the linear growth

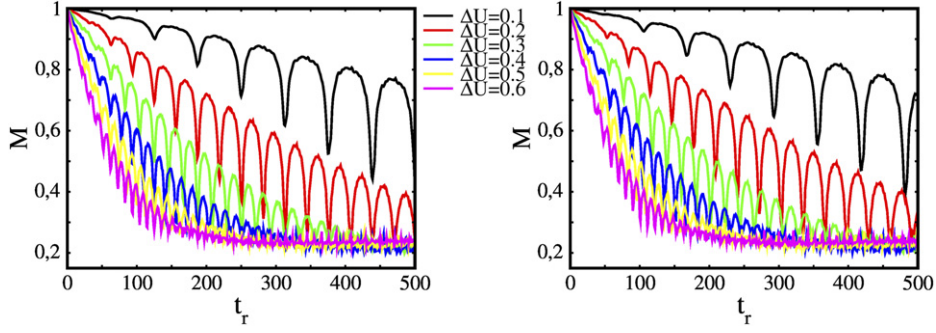


**Figure 4.** Loschmidt echo  $M = |\langle \psi(t=0) | \psi(t=2t_r) \rangle|^2$  as a function of  $t_r$ . (Left panel and right panel) Show the cases of  $U=0$  and  $U=2$  respectively with  $\Delta U = 0.1; 0.2; 0.3; 0.4; 0.5; 0.6$ . Other parameter values are the same as in figure 1.

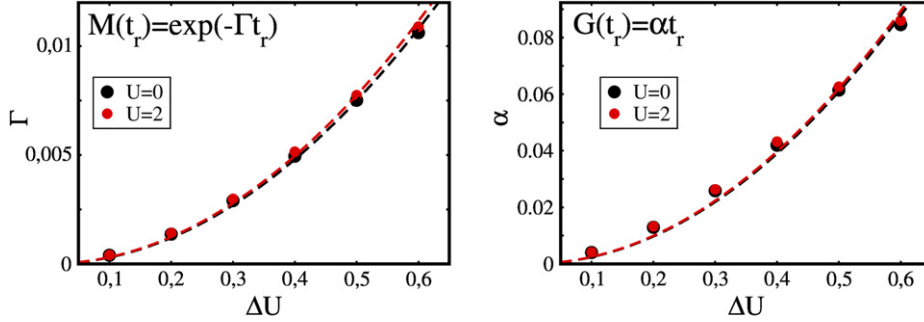


**Figure 5.** (Left) Exponential decay rate  $\Gamma$  of the Loschmidt echo vs  $\Delta U$  for  $U=0$  (black circles) and  $U=2$  (red circles); the values of  $\Gamma$  are obtained from the exponential fit  $M(t_r) = \exp(-\Gamma t_r)$  for  $t_r \in [0, 10/\Delta U]$  from the curves of figure 4. (Right) Linear growth rate of final entropy of entanglement  $G(t_r) = S(2t_r)$  vs  $\Delta U$  for  $U=0$  (black circles) and  $U=2$  (red circles); the values of  $\alpha$  are obtained from the linear fit  $G(t_r) = \alpha t_r$  for  $t_r \in [0, 10/\Delta U]$  from the curves of figure 3. The dashed curves in both panels show the fits of  $\Gamma$  and  $\alpha$  by square dependence on  $\Delta U$  (see text).

of  $G$  with time  $t_r$  and the proportionality of the growth rate  $\alpha \propto (\Delta U)^2$ , as the Fermi golden rule, is less obvious since this implies that the number of involved states grows exponentially with time  $t_r$ . We expect that the linear time dependence  $G = \alpha t_r$  (at small times) is in some way linked to an exponential spreading of the wave packet with time, which results from the positive classical Kolmogorov–Sinai entropy  $h$ . In fact for the classical chaotic dynamics  $h$  gives the entropy growth rate in time [5, 6]. In this context the perturbation  $\Delta U$  gives a quadratic correction to this rate.

We note that various properties of entropy of entanglement have been discussed in the literature, including links of its growth rate with the Kolmogorov–Sinai entropy (see e.g. references [53–57]). However, here we stress the properties of entanglement with respect to time reversal operation which is a certain new element in the context of entanglement studies.

Of course, there are various physical characteristics which are potentially interesting to study with respect to time reversal. However, a specific feature of time dependence of the

entropy of entanglement  $S(t)$  is that its change in time takes place only due to interactions which is the reason for its investigations here.

#### 4. Poincaré recurrences of entanglement

Here we consider the kicked rotator for two interacting particles with absorption. The time evolution is given by:

$$|\psi(t+1)\rangle = U_a U_{\text{KR}} |\psi(t)\rangle. \quad (10)$$

Here, the operator  $U_{\text{KR}}$  is given by (4)–(6) and the operator  $U_a$  represents absorption at the borders  $\pm L/2 = \pm N/4$ , i.e., it is a non-unitary operator which is diagonal in momentum representation and with eigenvalues being either 1 if  $-L/2 \leq p_1 < L/2$  and  $-L/2 \leq p_2 < L/2$  or 0 for all other cases. Due to the non-unitarity of this operator the survival probability  $P(t) = \|\psi(t)\|^2$  of both particles decays with time. In the following, we compute all quantities (except for  $P(t)$  itself) by first renormalizing the state  $|\psi(t)\rangle \rightarrow |\psi(t)\rangle / \|\psi(t)\|$ . This model was already extensively studied for the case of one particle in [38, 39, 42, 43].

We note that there are various interesting regimes of Poincaré recurrences of entanglement  $S(t)$  that requires presentation of various cases given in this section and next two sections. Additional results are also given in supplementary material.

We start with the initial entangled state:

$$|\psi(t=0)\rangle = \alpha_1(0)|u_1(0)\rangle \otimes |v_1(0)\rangle + \alpha_2(0)|u_2(0)\rangle \otimes |v_2(0)\rangle \quad (11)$$

with  $\alpha_1(0) = \alpha_2(0) = 1/\sqrt{2}$  and

$$|u_1(0)\rangle = |p_1 = 6\Delta p\rangle \quad (12)$$

$$|u_2(0)\rangle = |p_1 = 7\Delta p\rangle \quad (13)$$

$$|v_1(0)\rangle = |p_2 = 7\Delta p\rangle \quad (14)$$

$$|v_2(0)\rangle = |p_2 = 8\Delta p\rangle, \quad (15)$$

where  $N$  is the total system size which is chosen as a multiple of the minimal size 128 and  $\Delta p = N/128$  is a size dependent scaling factor. Here the state  $|p_j\rangle$  ( $j = 1, 2$ ) is the momentum eigenstate of particle  $j$  with integer (quantum) momentum values  $-N/2 \leq p_j < N/2$  and  $\hat{p}_j$  is the associated momentum operator of particle  $j$ . In particular, the states  $|u_{1,2}\rangle$  correspond to the first and the states  $|v_{1,2}\rangle$  correspond to the second particle.

In this and the following sections, we present in figures results for  $U = 0$  and  $U = 2$ ,  $U_r = 1$ . For this section, we have also computed additional results for other three interaction cases  $U = -2$ ,  $U_r = 1$  and  $U = \pm 2$ ,  $U_r = 0$  which are qualitatively similar. The corresponding data are not shown in figures but we mention in the discussions the important differences.

Concerning the parameters  $T$  and  $k$  we choose:  $T = \hbar$ ,  $k = K/\hbar$  with  $K = 7$  and  $\hbar$  is fixed by the condition that  $k = N/8$  implying  $\hbar = K/k = 56/N$ . The value  $K = 7$  corresponds to strong chaos with two small islands and has the particular feature that the classical decay (in case with of absorption at some border), described by the statistics of Poincaré recurrences, is also exponential in contrast to a typical subtle power law decay in presence of significant stable islands [45, 46, 58].

To compute numerically the application of the operator  $U_{\text{KR}}$  to the state  $|\psi(t)\rangle$  given in momentum representation we apply first the diagonal phase shift due to (a half of) the free rotation (the term (6)), transform the state to phase representation using a backward 2D-FFT,

apply the diagonal kick operator (the term (5)), transform the state back to momentum representation using a forward 2D-FFT, and then we apply the second half of the free rotation (the term (4)). In absence of interaction  $U = 0$ , it also possible to use 1D-FFT and one-particle operators for free rotation and the kick operator applied directly to the Schmidt states  $|u_{1,2}\rangle$  and  $|v_{1,2}\rangle$  (see also [33] for some technical details on this).

We note that in classical momentum units:  $p_{\text{cl}} = \hbar p_j$  the absorption border is  $p_{\text{max}} = \hbar L/2 = (56/N) \cdot N/4 = 14 = (2\pi) \cdot 2.228$  corresponding to 2.228 classical momentum cells in each direction (from 0 to  $\pm p_{\text{max}}$ ). The classical momentum values of the two states  $|u_2\rangle$  and  $|v_1\rangle$ , given in (13) and (14) and used in the initial state (11), correspond to:  $\hbar (7N/128) = (56/N) (7N/128) = 49/16 = (2\pi) \cdot 0.4874 \approx (2\pi) \cdot 0.5$ , which is in the middle of the classical cell in order to avoid the two small stable islands at  $p_{\text{cl}} = 0$  (and some non-trivial phase values). The other two states  $|u_1\rangle$  and  $|v_2\rangle$  are close by to  $|u_2\rangle$  or  $|v_1\rangle$  by a factor of 6/7 or 8/7 respectively.

Assuming a simple 1D classical diffusive process

$$\frac{\partial \rho_{\text{cl}}(p, t)}{\partial t} = D \frac{\partial^2 \rho_{\text{cl}}(p, t)}{\partial p^2} \quad (16)$$

for the classical density  $\rho_{\text{cl}}(p)$  (of one particle), with diffusion constant  $D = k^2/4 = N^2/256$  and absorption at  $p = \pm L/2 = \pm N/4$ , i.e., Dirichlet boundary conditions  $\rho_{\text{cl}}(\pm L/2) = 0$  at the absorption border, one can show that the classical survival probability (for one particle) decays (for long times) as  $P_1(t) \sim \exp(-t/t_{\text{Th}})$  with  $t_{\text{Th}} = L^2/(\pi^2 D) = 64/\pi^2 \approx 6.4846$  being the Thouless time. For both particles we expect  $P(t) = P_1^2(t)$  such that  $P(t)^{1/2} \sim \exp(-t/t_{\text{Th}})$ .

When applying the quantum iteration (10), the state at a given (integer) iteration time  $t$  takes the more general form (after renormalization):

$$|\psi(t)\rangle = \sum_{i=1}^L \alpha_i(t) |u_i(t)\rangle \otimes |v_i(t)\rangle. \quad (17)$$

We describe in appendix A.1 some details on the practical computation of the general Schmidt decomposition and also some other related properties. Furthermore, we also show in appendix A.2, that in absence of interaction there is indeed a more efficient numerical scheme to recompute the Schmidt decomposition and in particular at arbitrary time  $t$  there are only two non-vanishing singular values being  $\alpha_1$  and  $\alpha_2$  and  $\alpha_i = 0$  for  $i = 3, \dots, L$  (note that the effective matrix size of  $\psi(p_1, p_2)$  is  $L \times L$  with  $L = N/2$  due to the absorption process).

Using the singular values one can compute the entropy of entanglement defined as [30]:

$$S(t) = -\text{Tr}[\rho_j \log_2(\rho_j)] = -\sum_{i=1}^L \alpha_i^2(t) \log_2[\alpha_i^2(t)] \quad (18)$$

(for either  $j = 1$  or  $j = 2$ ). In this definition we use the logarithm with respect to the base 2 such that the entropy of the initial state (11) is exactly  $S(t = 0) = 1$ .

For  $U = 0$ , we stop the iteration when  $|u_1\rangle$  converges (up to a global phase factor) with an error below  $10^{-12}$  (for the norm of the difference vector with proper phase) between two time steps (and then we also iterate up to the next power of two for the iteration time).

For  $U \neq 0$ , we stop the quantum interaction when the change of entropy between two time steps is below  $10^{-14}$  (and then we iterate up to the next power of two for the iteration time). It turns that for the two cases with  $U_r = 1$  also the state  $|\psi(t)\rangle$  converges up to a global phase factor to a limit state  $|\psi_\infty\rangle$ , i.e.,  $|\psi(t)\rangle \rightarrow e^{i\phi(t)} |\psi_\infty\rangle$  for  $t \rightarrow \infty$  with a time dependent phase

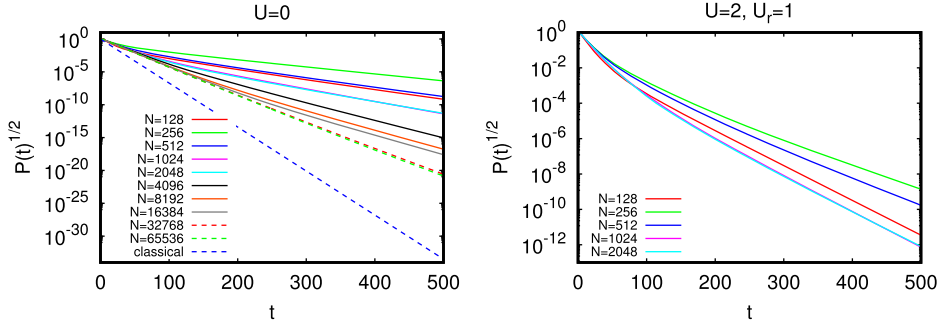


**Figure 6.** (Left) Decay of  $P(t)^{1/2} = \|\psi(t)\|$  where the norm is obtained before renormalization of the state  $|\psi(t)\rangle$  for interaction value  $U = 0$  and system size  $128 \leq N \leq 65\,536$ . The dashed blue line shows the classical decay corresponding to  $P(t)^{1/2} = \exp(-t/t_{\text{Th}})$  (for two particles) and with  $t_{\text{Th}} = 64/\pi^2 \approx 6.4846$  being the Thouless time. (Right) Decay of  $P(t)^{1/2} = \|\psi(t)\|$  for interaction values  $U = 2, U_r = 1$  and system size  $128 \leq N \leq 2048$ . The curves for  $N = 1024$  (pink) and  $N = 2048$  (cyan) are very close.

factor. This is coherent with the picture that the non-unitary iteration operator  $U_a U_{\text{KR}}$  has complex eigenvalues of the form  $\exp(-\gamma_i/2 + i\omega_i)$  with  $0 < \gamma_1 < \gamma_2 < \dots$  and that  $|\psi_\infty\rangle$  is the eigenvector of the leading mode with absorption rate  $\gamma_1$  and furthermore the time dependent phase factor is  $\phi(t) = \omega_1 t + \text{const}$ . For  $U_r = 1$  this convergence is rather fast and comparable in speed to the convergence of the entropy. However, for  $U_r = 0$  this convergence to the limit state is quite slower. We have also verified that for  $U = 0$  the general method of computing all singular values, suitable for arbitrary  $U$  values, produces the same results (up to numerical precision) as the more efficient method explained in appendix A.2.

Figure 6 shows the quantity  $P(t)^{1/2}$  obtained from the quantum iteration (10) for the two cases  $U = 0$  with system size  $128 \leq N \leq 65\,536$  (left panel) and the interaction case  $U = 2, U_r = 1$  with system size  $128 \leq N \leq 2048$  (right panel). In the left panel also the classical decay based on the model of simple classical diffusion is shown. For  $U = 0$  the quantum decay is for long time scales strongly reduced with respect to the classical decay and this effect is strongest for small values of  $N$ . For larger values of  $N$  the time scale where the semiclassical limit is valid increases as can be seen from the two curves for  $N = 32\,768$  and  $N = 65\,536$ . However, even for this semiclassical quantum decay the exponential decay time is by a factor  $\sim 1.6$  longer than the classical Thouless time. This can be explained by the fact that the simple diffusive model is not very accurate on a quantitative level due to the small number of classical cells ( $\sim 4.5$  in total). In this case, despite the strong chaos for  $K = 7$ , the effects of the classical phase space structure may cause significant deviations with respect to the simple diffusive model. For the interaction case, the decay visible for the more modest system sizes up to  $N = 2048$  is comparable to the decay for  $U = 0$  at same system size values. This also holds for the other interaction cases not shown in the figure.

Figure 7 shows for  $U = 0$  and different values of  $N$  the decay of the entropy of entanglement  $S(t)$  which converges to 0 for  $t \rightarrow \infty$  for all cases. However, the exponential decay rates for long time scales vary strongly with system size in a non-systematic way, e.g., the long time decay for  $N = 32\,768$  is significantly slower than for the other cases. Furthermore, even for a case with strong long time decay, the onset of this decay may be quite late, e.g., for  $N = 65\,536$  the entropy is rather constant close to unity for  $t \leq 500$  with values clearly above the data for most of the other cases and starts to decay quite strongly at  $t \approx 1000$  with final values clearly below the values for several of the other cases.

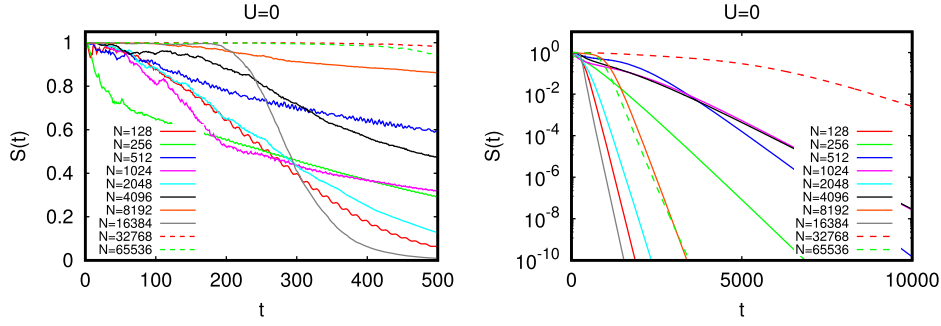


**Figure 7.** (Left) Decay of the entropy of entanglement  $S(t)$  for interaction value  $U = 0$  and system size  $128 \leq N \leq 65\,536$ . (Right) As left panel but using a logarithmic scale for the entropy and an increased time range.

In particular, we find that  $\alpha_1(t) \rightarrow 1$  and  $\alpha_2(t) \rightarrow 0$  for  $t \rightarrow \infty$  and (up to phase factors)  $|v_1(t)\rangle = |u_1(t)\rangle$  and  $|v_2(t)\rangle = |u_2(t)\rangle$ . (See below for the corresponding Husimi functions for some examples.) In absence of interaction the non-unitary iteration operator is simply a tensor product of two independent (and identical) one-particle non-unitary iteration operators:  $U_a U_{\text{KR}} = (U_a^{(1)} U_{\text{KR}}^{(1)}) \otimes (U_a^{(2)} U_{\text{KR}}^{(2)})$ . During the time iteration both  $|u_1(t)\rangle$  and  $|v_1(t)\rangle$  converge to the leading eigenvector of the one-particle non-unitary iteration operator and the long time decay of the survival probability (of both particles) is simply  $P(t) \sim \exp(-2\gamma_1^{(1)}t)$  where  $\gamma_1^{(1)}$  is the absorption rate of this leading eigenvector. However, after global renormalization, the entropy is determined by  $\alpha_2$  via

$$S(t) \approx -\alpha_2^2 \log_2(\alpha_2^2) - \alpha_1^2 \log_2(\alpha_1^2) \approx -\alpha_2^2 \log_2(\alpha_2^2) + \alpha_2^2 / \ln(2) \quad (19)$$

for  $\alpha_2 \ll 1$  since  $\alpha_1^2 = 1 - \alpha_2^2$ . We expect that  $\alpha_2 \sim \exp[-(\gamma_2^{(1)} - \gamma_1^{(1)})t]$  where  $\gamma_2^{(1)}$  is the absorption rate of the second eigenvector (of the non-unitary one-particle iteration operator) which is  $\sim |v_2(t)\rangle = |u_2(t)\rangle$  (up to a phase factor) for  $t \rightarrow \infty$ . Therefore, the entropy should decay as:

$$S(t) \sim \left( (\gamma_2^{(1)} - \gamma_1^{(1)})t + \text{const.} \right) \exp[-2(\gamma_2^{(1)} - \gamma_1^{(1)})t]. \quad (20)$$

For  $U = 0$  and  $N = 1024$ , we obtain from exponential fits of  $P(t)$  and  $\alpha_2(t)$  that  $\gamma_1^{(1)} = 0.042\,1459$  and  $\gamma_2^{(1)} - \gamma_1^{(1)} = 0.001\,060\,19$  (with virtually no statistical fit error for both quantities) and also (20) is numerically very well confirmed. The inverse of  $\gamma_1^{(1)}$  provides the decay time  $t_q \approx 23.73$  which is about 3.66 times larger than the classical decay time  $t_{\text{Th}} = 64/\pi^2 = 6.4846$  (see also pink full line and blue dashed line in the left panel of figure 6).

Figure 8 shows the behavior of the entropy  $S(t)$  for the case of  $U = 2$ ,  $U_r = 1$  and system size  $128 \leq N \leq 2048$ . Initially the entropy increases to maximum values between  $S_{\text{max}} \approx 4.2$  at  $t \approx 25$  (for  $N = 128$ ) and  $S_{\text{max}} \approx 3.0$  at  $t \approx 50$  (for  $N = 2048$ ) and then it decays for  $t \rightarrow \infty$  exponentially to a limit value  $S_\infty$  which is significantly larger than unity and slightly below 2. The values of  $S_\infty$  for each case of  $N$  are also given in the right panel of figure 8 which shows the (modulus of the) difference  $S(t) - S_\infty$  versus time on a longer time scale and logarithmic scale for the vertical axis. One also observes that for long time scales there are small amplitude oscillations of  $S(t)$  around  $S_\infty$ .

The behavior for the case  $U = -2$ ,  $U_r = 1$  (not shown in the figure) is qualitatively similar with an initial increase of  $S(t)$  and similar maximum values and with slightly different values

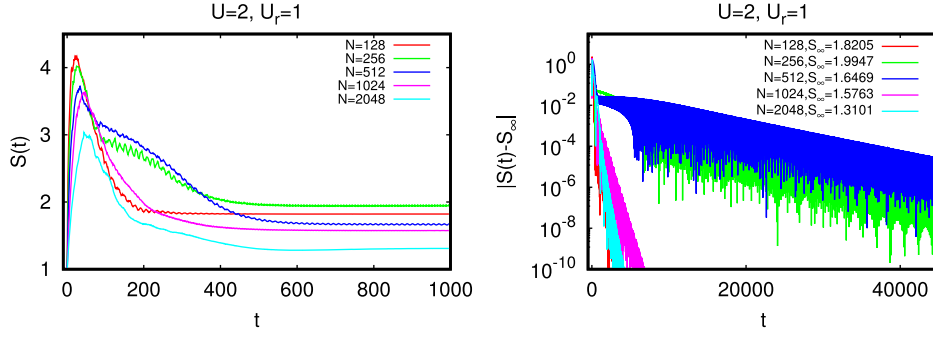


**Figure 8.** (Left) Entropy of entanglement  $S(t)$  versus iteration time for interaction values  $U = 2$ ,  $U_r = 1$  and system size  $128 \leq N \leq 2048$ . (Right) Decay of the difference  $|S(t) - S_\infty|$  for the same values of interaction and system size with  $S_\infty = \lim_{t \rightarrow \infty} S(t)$ . The shown time scale is increased and a logarithmic scale for the vertical axis is used. The modulus of the difference is taken because  $S(t)$  is for certain time values  $t$  below the limit value due to small amplitude oscillations for long time scales. The value of  $S_\infty$  is significantly larger than unity.

of  $S_\infty$ . However, the decays for the two cases of  $N = 256$  and  $N = 512$  are significantly faster with a convergence time scale for  $S(t)$  at  $t_{\max} \approx 9000$  or  $3000$  respectively (the other two cases  $N = 128$  and  $N = 1024$  have similar values of the convergence time as for  $U = 2$ ,  $U_r = 1$  and visible in figure 8).

For the two cases of  $U = \pm 2$ ,  $U_r = 0$  (not shown in the figure) the limit value is precisely  $S_\infty = 1$  and it turns out that the limit state has only two non-vanishing singular values  $\alpha_1 = \alpha_2 = 1/\sqrt{2}$  while  $\alpha_i = 0$  for  $i \geq 3$ . However, also here the entropy initially increases to the maximum values between  $S_{\max} \approx 3.5$  at  $t \approx 25$  (for  $N = 128$ ) and  $S_{\max} \approx 2.5$  at  $t \approx 25$  (for  $N = 512$ ) and with  $S_{\max} \approx 2.6$  at  $t \approx 50$  (for  $N = 1024$ ). At these intermediate iteration times also the singular values  $\alpha_i$  for  $i \geq 3$  provide significant contributions to the state  $|\psi(t)\rangle$ . The decay of  $S(t) - S_\infty$  for  $t \rightarrow \infty$  is here very close to a pure exponential decay without any amplitude oscillations (except for  $N = 1024$  with some deviations from the pure exponential behavior) and with a convergence time scale of  $t_{\max}$  between  $300$  (for  $N = 128$ ) and  $t_{\max}$  between  $2400$  (for  $N = 1024$ ) such that  $S(t) - S_\infty < 10^{-10}$  for  $t > t_{\max}$ .

For  $U = \pm 2$ ,  $U_r = 1$  all singular values contribute to the limit state as can be seen in figure 9 (for  $U = 2$ ,  $U_r = 1$ ; the other case  $U = -2$ ,  $U_r = 1$  being very similar). However the first two singular values  $\alpha_1 = \alpha_2 \approx 0.66$ – $0.69$  (see caption of figure 9 for more precise values) are dominant while  $\alpha_i \leq 0.1$  for  $i \geq 3$ . Furthermore the singular values of the limit state appear in degenerate pairs. This is due to the fact that for all four interaction cases the limit state is anti-symmetric with respect to particle exchange and a general property for the singular values of a complex skew-symmetric matrix [61] (see also appendix A.1 for some explanations on this).

We show in supplementary material (SupMat) that the weight of the symmetric component of the wavefunction decays exponentially to zero (see figure S1) for long time scales.

We have also computed for  $U = 0$  and the interaction cases the first Schmidt vectors  $|u_{1,2}\rangle$ ,  $|v_{1,2}\rangle$  and the associated Husimi functions (see e.g. [33, 59, 60] for details on the definition and computation of Husimi functions). The vectors  $|u_{1,2}\rangle$  for  $U = 0$  and  $U = 2$ ,  $U_r = 1$  (all for  $N = 1024$ ) are shown in figure 10 for three time values being  $t = 1$ ,  $t = 4$  and some very long time being  $t = t_{\max} = 16\,384$  for  $U = 0$  or  $t = t_{\max} = 4096$  for  $U = 2$ ,  $U_r = 1$ . For  $t = 1$ ,

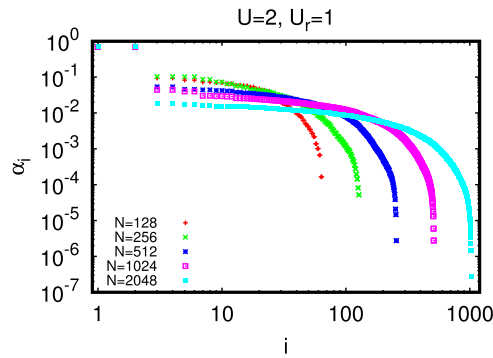


**Figure 9.** Singular values  $\alpha_i$  (appearing in the Schmidt decomposition of the limit state  $\lim_{t \rightarrow \infty} |\psi(t)\rangle$ ) versus index  $i$  for interaction values  $U = 2$ ,  $U_r = 1$  and system size  $128 \leq N \leq 2048$ . Both axis are shown on a logarithmic scale. The singular values appear in degenerate pairs since the limit state is anti-symmetric with respect to particle exchange. The values of the top pair of singular values are  $\alpha_1 = \alpha_2 = 0.671\,52, 0.663\,17, 0.685\,10, 0.689\,65, 0.699\,24$  for  $N = 128, 256, 512, 1024, 2048$  respectively.

these states occupy the same manifold but for the two interaction cases the densities at some positions on this manifold are reduced in comparison to the non-interacting case.

For  $t = 4$  the phase space structure is quite complicated but rather similar between the interacting and non-interacting cases for both states  $|u_{1,2}\rangle$ . At long times the state  $|u_1\rangle$  of  $U = 0$  is very close to the state  $|u_2\rangle$  of  $U = 2$ ,  $U_r$  and similarly between  $|u_2\rangle$  of  $U = 0$  and  $|u_1\rangle$  of  $U = 2$ ,  $U_r = 1$ .

The states  $|v_{1,2}\rangle$  are not shown but for long times they are determined by  $|u_{1,2}\rangle$  depending on the interaction: for  $U = 0$  they are given by:  $|u_1\rangle = |v_1\rangle$  and  $|u_2\rangle = |v_1\rangle$  (up to phase factors), or more explicitly:

$$|\psi_\infty\rangle = C_1 \alpha_1 |u_1\rangle \otimes |u_1\rangle + C_2 \alpha_2 |u_2\rangle \otimes |u_2\rangle, \quad (21)$$

where  $\alpha_1 \approx 1, \alpha_2 = \sqrt{1 - \alpha_1^2} \ll 1$  and  $C_1, C_2$  represent unknown (and time dependent) phase factors.

For  $U = \pm 2$  and  $U_r = 0, 1$  we have a different situation where (up to a global phase factor)  $|v_1\rangle = |u_2\rangle$  and  $|v_2\rangle = -|u_1\rangle$  which is confirmed by the Husimi functions of these states and the sign is due to the established anti-symmetry of the limit state, or more explicitly:

$$|\psi_\infty\rangle = C \alpha_1 (|u_1\rangle \otimes |u_2\rangle - |u_2\rangle \otimes |u_1\rangle) + \alpha_3(\dots) + \dots \quad (22)$$

where  $\alpha_1 = \alpha_2 \approx 0.7$ ,  $C$  is an unknown phase factor and (for  $U_r = 1$ ) there are also smaller contributions due to  $\alpha_i$  for  $i \geq 3$ .

As already discussed above, the limit state (21) for  $U = 0$  has a decay rate  $\gamma_1^{(1)} = 0.042\,1459$  (for  $N = 1024$ ) since both modes  $|u_1\rangle = |v_1\rangle$  in the first term have the decay rate  $\gamma_1^{(1)}/2$  (of the non-interacting one-particle iteration operator). For the anti-symmetric state (22) in presence of interaction, neglecting the contributions of  $\alpha_i$  for  $i \geq 3$  and assuming that  $|u_{1,2}\rangle$  represent well the first two decay modes of the non-interacting one-particle iteration operator, one would expect a decay rate of  $(\gamma_1^{(1)} + \gamma_2^{(1)})/2 = 0.042\,6760$  where  $\gamma_2^{(1)}$  is extracted from the difference  $\gamma_2^{(1)} - \gamma_1^{(1)} = 0.001\,060\,19$  which is according to the discussion above just the decay rate of  $\alpha_2(t)$  at  $U = 0$ .

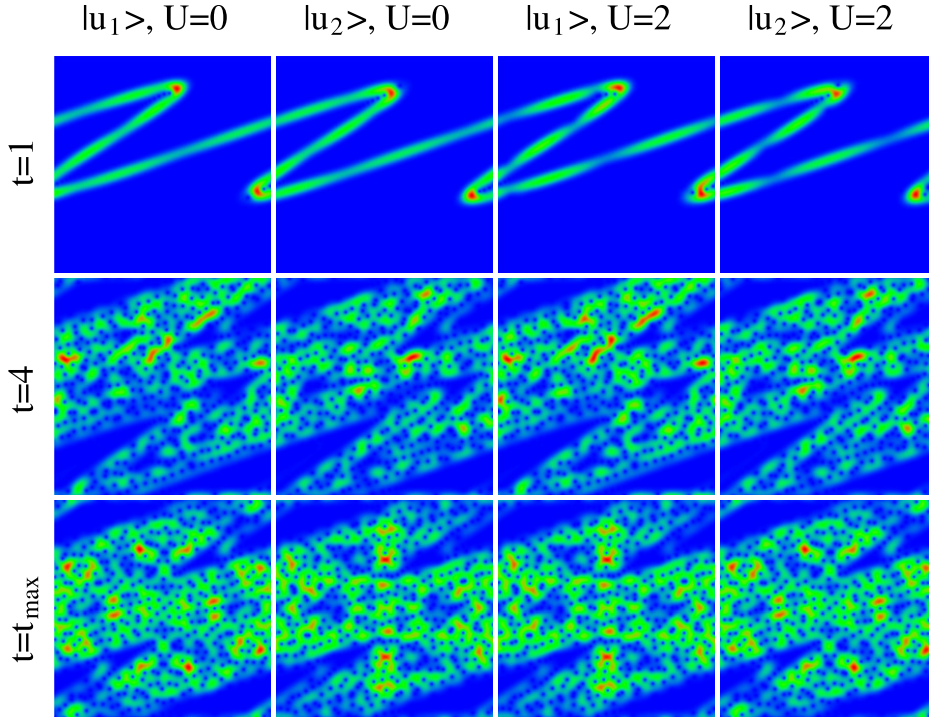


**Figure 10.** Husimi functions of the Schmidt states  $|u_1\rangle$ ,  $|u_2\rangle$ , for  $U = 0$  or  $U = 2$  (with  $U_r = 1$ ) and  $N = 1024$  at three iteration times  $t = 1$ ,  $t = 4$  and  $t = t_{\max}$  with  $t_{\max} = 16\,384$  for  $U = 0$  or  $t_{\max} = 4096$  for  $U = 2$ . The horizontal axis corresponds to the phase  $\theta \in [-\pi, \pi]$  and the vertical axis to the momentum  $p_{cl} \in [-p_{\max}, p_{\max}]$  where  $p_{\max} = (2\pi) \cdot 2.228$  is the momentum absorption border in classical units. The colors red/green/blue correspond to maximal/medium/minimal values of the Husimi function.

Numerically, we find that the decay rates of the limit state in presence of interaction (for  $U_r = 1$ ) are  $\gamma_1^{(U=2, U_r=1)} = 0.045\,5464$  and  $\gamma_1^{(U=-2, U_r=1)} = 0.045\,960$ . Even though these values are quite close to the above expectation the difference is still 2 or 3 times larger than  $\gamma_2^{(1)} - \gamma_1^{(1)}$ , indicating that the interaction has a significant influence on the decay rate as such (in addition to ‘imposing’ the anti-symmetric limit state (22)). This is also plausible since for  $U_r = 1$  the contributions of the other singular values  $\alpha_i$  for  $i \geq 3$  are still quite important which can be seen from the limit value of  $S_\infty$  which is closer to 2 than to 1.

However, for the short range interaction  $U_r = 0$  we have:  $\gamma_1^{(U=\pm 2, U_r=0)} = 0.042\,64947$  which is indeed very close to the theoretical expectation (difference being the fraction  $1/40$  of  $\gamma_2^{(1)} - \gamma_1^{(1)}$ ). For this case, the interaction is responsible for the anti-symmetric combination of the first two terms in (22) but has otherwise no strong effect on the decay. This is also coherent with the fact that for this case  $\alpha_i = 0$  for  $i \geq 3$  (for the limit state at  $t \rightarrow \infty$ ).

One should note that for pairwise degenerate singular values the Schmidt decomposition is not unique and does not change if one applies to  $|u_{1,2}\rangle$  and  $|v_{1,2}\rangle$  an arbitrary  $2 \times 2$  unitary rotation (same rotation for both pairs). Therefore, the numerical procedure that computes the Schmidt vectors selects in some random way the precise choice of these vectors. However, despite this degree of liberty we have been able to verify that essentially the vectors

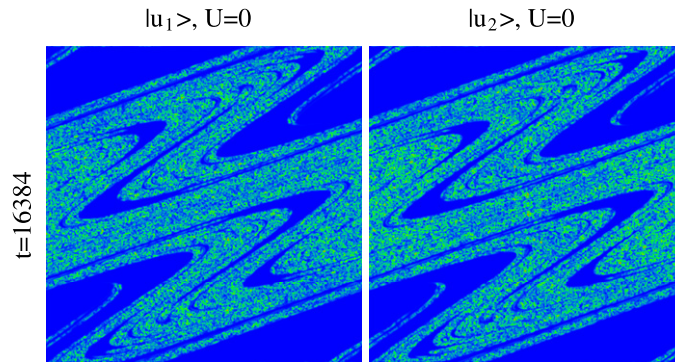


**Figure 11.** Husimi functions of the Schmidt states  $|u_1\rangle, |u_2\rangle$ , for  $U = 0$  and  $N = 65\,536$  at final iteration time  $t = 16\,384$ . The signification of both axes and the color codes is the same as in figure 10.

$|u_{1,2}\rangle$  in the limit  $t \rightarrow \infty$  for  $U = 0$  coincide roughly with the first two Schmidt vectors for the four interaction cases. For  $U_r = 0$  there are no other Schmidt components but for  $U_r = 1$  there are with a modest weight further Schmidt components due to the interaction which also provide a quite significant influence on the decay rate. Apparently, the interaction imposes essentially an anti-symmetric limit state where both particles occupy the first two non-interacting absorption modes in an anti-symmetric entangled combination. However, for  $U_r = 1$  the other Schmidt components also have a significant weight in the entropy of entanglement which is closer to 2 than to 1.

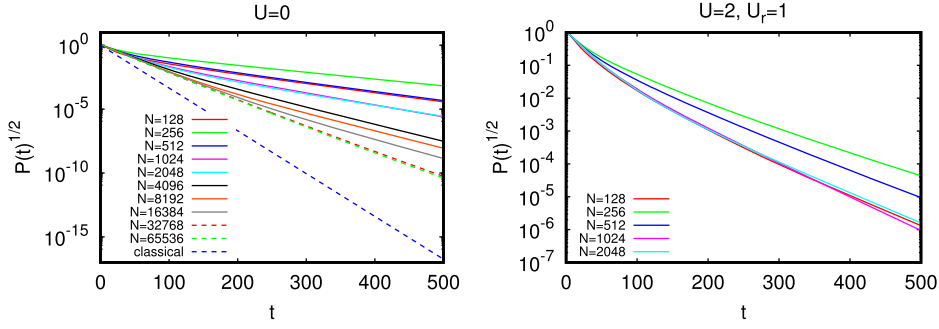
In figure 11, we also show the Husimi functions of  $|u_{1,2}\rangle$  for  $U = 0$  and a larger system size  $N = 65\,536$  at final iteration time  $t = 16\,384$ . The overall phase space structure of these modes is rather complicated but there are some positions, with very small red dots, where the density is locally enhanced. The Husimi function has a fractal structure corresponding to a fractal repeller of non-escaping classical orbits (compare with the one-particle case discussed in [43]).

### 5. Poincaré recurrences of entanglement with absorption of one particle

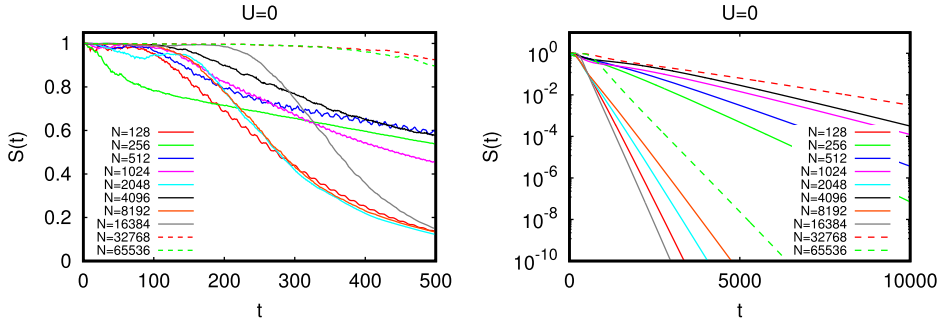
In this section, we consider a different case with the same time evolution as in the previous section (exact same parameters; in particular  $K = 7$ ) but the absorption at the absorption border is applied only to the second particle while the first particle can move in the full available phase space (with periodic boundary conditions) and is never absorbed. We call this the asymmetric absorption case (in contrast to the symmetric absorption case of the previous section).

Figure 12 shows for this case the quantity  $P(t)^{1/2}$  obtained from the quantum iteration (10) for  $U = 0$  with system size  $128 \leq N \leq 65\,536$  (left panel) and the interaction case  $U = 2$ ,  $U_r = 1$  with system size  $128 \leq N \leq 2048$  (right panel). In the left panel also the classical decay based on the model of simple classical diffusion (with absorption for only the second particle) is shown.

The results shown in figure 12 are very similar to the results of figure 6 if one takes into account that all decay times are increased by a factor of 2, i.e. we have roughly  $P_{AS}(t) \approx P(t/2)$  where  $P_{AS}(t)$  is a curve of figure 12 for the asymmetric absorption of only the second particle and  $P(t)$  is a curve of figure 6 for the absorption of both particles.



**Figure 12.** (Left) Decay of  $P(t)^{1/2} = \|\psi(t)\|$  where the norm is obtained before renormalization of the state  $|\psi(t)\rangle$  for interaction value  $U = 0$ , system size  $128 \leq N \leq 65\,536$  and absorption only for the second particle. The dashed blue line shows the classical decay corresponding to  $P(t)^{1/2} = \exp(-t/(2t_{\text{Th}}))$  (for *one* particle) and with  $t_{\text{Th}} = 64/\pi^2 \approx 6.4846$  being the Thouless time. (Right) Decay of  $P(t)^{1/2} = \|\psi(t)\|$  for interaction values  $U = 2$ ,  $U_r = 1$  and system size  $128 \leq N \leq 2048$ .



**Figure 13.** (Left) Decay of the entropy of entanglement  $S(t)$  for interaction value  $U = 0$ , system size  $128 \leq N \leq 65\,536$  and absorption only for the second particle. (Right) As left panel but using a logarithmic scale for the entropy and an increased time range.

Figure 13 shows for the case of asymmetric absorption,  $U = 0$  and different values of  $N$  the decay of the entropy of entanglement  $S(t)$  which converges also to 0 for  $t \rightarrow \infty$  for all cases. Qualitatively the overall (rather complicated) behavior is similar to the case of symmetric absorption shown in figure 7, i.e. the decay times depend in a non-systematic way on  $N$ , sometimes with a late onset of the decay. However, cases for slow, fast or late decay happen for the same values of  $N$  as in figure 7.

We find again that  $\alpha_1(t) \rightarrow 1$  and  $\alpha_2(t) \rightarrow 0$  for  $t \rightarrow \infty$ . The state  $|v_1(t)\rangle$  is now of course different from  $|u_1(t)\rangle$  but it is identical (up to a phase factor) for  $t \rightarrow \infty$  to the state  $|v_1(t)\rangle$  for the case of symmetric absorption while  $|u_1(t)\rangle$  corresponds to the free (ergodic) quantum evolution of the first particle. (See below for the corresponding Husimi functions for some examples.)

The efficient computation method for  $U = 0$  (see appendix A.1) is also valid here. However, the triangular  $2 \times 2$  matrix  $R_u$  associated to the first particle is now always the unity matrix since no orthogonalization procedure for the states  $|u_{1,2}\rangle$  is necessary during the iteration (or in other words if it is done anyway one simply obtains for  $R_u$  the unit matrix).

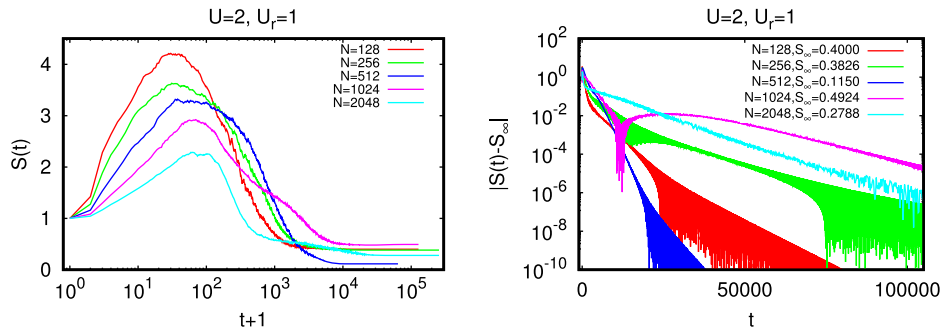


**Figure 14.** (Left) Entropy of entanglement  $S(t)$  versus iteration time for interaction values  $U = 2$ ,  $U_r = 1$ , system size  $128 \leq N \leq 2048$  and absorption only for the second particle. The horizontal axis is shown in logarithmic scale for  $(t + 1)$  (in order to keep the first data point at  $t = 0$  visible). (Right) Decay of the difference  $|S(t) - S_\infty|$  for the same values of interaction and system size with  $S_\infty = \lim_{t \rightarrow \infty} S(t)$ . The shown time scale is linear and a logarithmic scale for the vertical axis is used. The modulus of the difference is taken because  $S(t)$  is for certain time values  $t$  below the limit value due to small amplitude oscillations for long time scales. The value of  $S_\infty$  is significantly smaller than unity.

However, the other matrix  $R_v$  for the second particle has a non-trivial behavior and therefore the Schmidt decomposition still evolves in a non-trivial way similar to the scheme described in appendix A.1.

The state  $|u_1(t)\rangle$  at arbitrary time  $t$  is a linear combination of both initial states  $|u_{1,2}(t = 0)\rangle$  to which the free one-particle kicked rotator time evolution is applied but the coefficients of this linear combination depend on the way the second particle is absorbed (by the successive products of the matrix  $R_v$ ). This situation is quite similar to the case of measurement of the second particle at some specific  $p_2$  values studied in [33] since such a measurement process can be viewed as an extreme case of absorption for all  $p_2$  values being different from the measured value.

Figure 14 shows for the asymmetric absorption case the behavior of the entropy  $S(t)$  for the case of  $U = 2$ ,  $U_r = 1$  and system size  $128 \leq N \leq 2048$ . Initially the entropy increases to maximum values between  $S_{\max} \approx 4.2$  at  $t \approx 25$  (for  $N = 128$ ) and  $S_{\max} \approx 2.3$  at  $t \approx 60$  (for  $N = 2048$ ) and then it decays for  $t \rightarrow \infty$  exponentially to a limit value  $S_\infty$  which is now significantly smaller than unity (but larger than zero). The values of  $S_\infty$  for each case of  $N$  are also given in the right panel of figure 14 which shows the (modulus of the) difference  $S(t) - S_\infty$  versus time on a longer time scale and logarithmic scale for the vertical axis. As in the case of symmetric absorption one also observes that for long time scales there are small amplitude oscillations of  $S(t)$  around  $S_\infty$ . However, now the convergence of the entropy is considerably slower than for the symmetric absorption case shown in figure 8, especially for  $N = 1024$  and  $N = 2048$ .

For  $U = 2$ ,  $U_r$  and the asymmetric absorption, also all singular values contribute to the limit state as can be seen in figure 15. However, now, due to the obvious absence of antisymmetry in the limit state (with respect to particle exchange) the singular values are no longer pairwise degenerate and the top singular value  $\alpha_1 \approx 0.98-0.99$  (see caption of figure 15 for more precise values) is dominant while  $\alpha_i < 0.062$  for  $i \geq 2$  (and  $N = 1024$ ). However, despite the dominating first singular value the resulting entropy (of the limit state) is still considerably larger than zero with values  $\approx 0.3-0.5$  (except for  $N = 512$  where the limit value is  $\approx 0.1$ ).

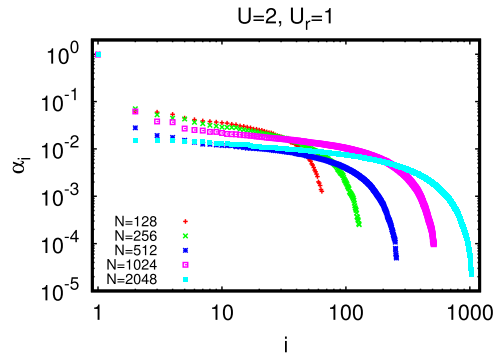


**Figure 15.** Singular values  $\alpha_i$  (appearing in the Schmidt decomposition of the limit state  $\lim_{t \rightarrow \infty} |\psi(t)\rangle$ ) versus index  $i$  for interaction values  $U = 2$ ,  $U_r = 1$ , system size  $128 \leq N \leq 2048$  and absorption only for the second particle. Both axis are shown on a logarithmic scale. The values of the top singular value are  $\alpha_1 = 0.98186, 0.98337, 0.99612, 0.98136, 0.99107$  for  $N = 128, 256, 512, 1024, 2048$  respectively.

As in the last section, we have also computed for  $U = 0$  and the interaction cases the first Schmidt vectors  $|u_{1,2}\rangle, |v_{1,2}\rangle$  and the associated Husimi functions [33, 59, 60]. The vectors  $|u_1(t)\rangle, |v_1(t)\rangle$  for  $U = 0$  and  $U = 2, U_r = 1$  (all for  $N = 1024$ ) are shown in figure 16 for three time values being  $t = 1, t = 4$  and some very long time being  $t = t_{\max} = 16384$  for  $U = 0$  or  $t = t_{\max} = 131072$  for  $U = 2, U_r = 1$ . Again for  $t = 1$ , these states occupy the same manifold but for the two interaction cases the densities at some positions on this manifold are reduced in comparison to the non-interacting case. (Note that the available phase space for  $|v_1(t)\rangle$  is reduced by a factor of 2 concerning the maximal  $p$  value as compared to  $|u_1(t)\rangle$ .)

Again for  $t = 4$  the phase space structure is quite complicated but rather similar between the interacting and non-interacting cases for both states  $|u_1\rangle$  and  $|v_1\rangle$  respectively.

At long times the state  $|u_1\rangle$  of  $U = 0$  seems to be ergodic while the state  $|v_1\rangle$  coincides (quite exactly and for both  $U = 0$  and  $U = 2, U_r = 1$ ) with the state  $|v_1\rangle$  for the symmetric absorption case ( $U = 0$ ) visible in figure 10 (see  $|u_1\rangle$  in this figure which coincides with  $|v_1\rangle$  for the symmetric absorption case at  $U = 0$ ). However, for  $U = 2, U_r = 1$  the state  $|u_1\rangle$  (at long times) is quite strange with a strongly enhanced probability in the absorption area  $|p| > p_{\max}$  of the other particle. Furthermore, also in the region  $|p| < p_{\max}$  the first particle has larger (smaller) probability values at classical positions where the second particle is absent (present). This indicates that the first particle is somehow repelled by the interaction from the second particle which cannot enter the absorption area and which is in a quite stable limit state  $|v_1\rangle$ .

In figure 17, we also show for the asymmetric absorption case the Husimi functions of  $|u_1\rangle$  and  $|v_1\rangle$  for  $U = 0$  and a larger system size  $N = 65536$  at final iteration time  $t = 16384$ . Similarly to the case  $N = 1024$  the state  $|u_1\rangle$  is ergodic and  $|v_1\rangle$  coincides (quite precisely) with the corresponding state for the symmetric absorption case (see state  $|u_1\rangle$  of figure 11). The Husimi function of the second absorbed particle has a fractal structure corresponding to a fractal repeller of non-escaping classical orbits, while the Husimi function of the first particle is homogeneous in the phase space.

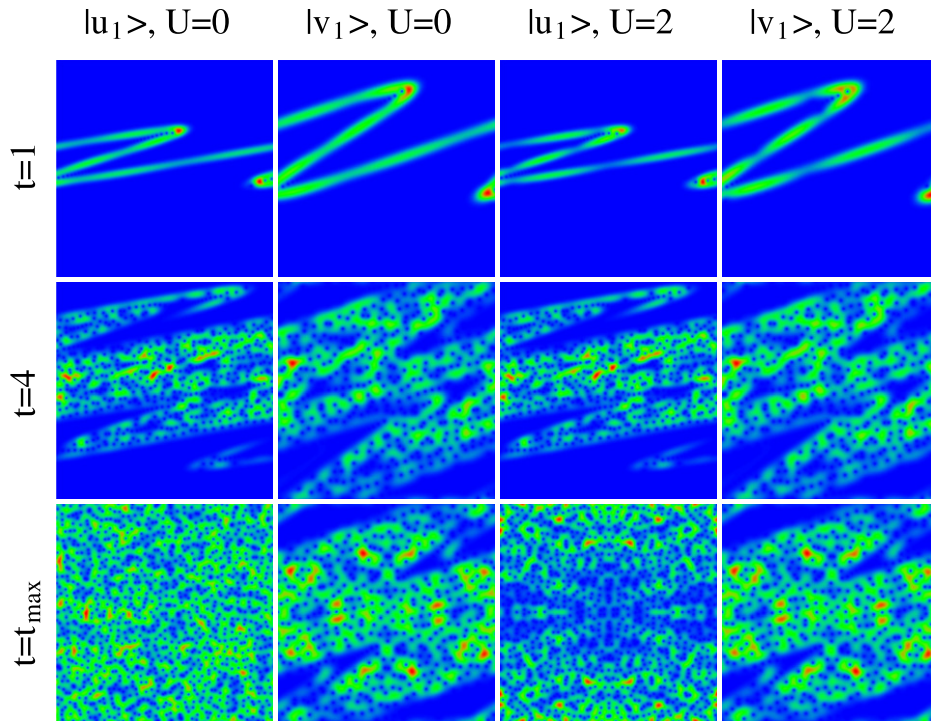


**Figure 16.** Husimi functions of the Schmidt states  $|u_1\rangle$ ,  $|v_1\rangle$ , for  $U = 0$  or  $U = 2$  (with  $U_r = 1$ ),  $N = 1024$  and absorption only for the second particle at three iteration times  $t = 1$ ,  $t = 4$  and  $t = t_{\max}$  with  $t_{\max} = 16\,384$  for  $U = 0$  or  $t_{\max} = 131\,072$  for  $U = 2$ . The horizontal axis corresponds to the phase  $\theta \in [-\pi, \pi]$  and the vertical axis to the momentum  $p_{cl} \in [-2p_{\max}, 2p_{\max}]$  (for  $|u_1\rangle$ ) or  $p_{cl} \in [-p_{\max}, p_{\max}]$  (for  $|v_1\rangle$ ) where  $p_{\max} = (2\pi) \cdot 2.228$  is the momentum absorption border in classical units (for the second particle) and  $2p_{\max}$  is the maximal classical momentum value for the full phase space in absence of absorption (for the first particle). The colors red/green/blue correspond to maximal/medium/minimal values of the Husimi function.

## 6. Poincaré recurrences of entanglement with absorption of one particle for $K = 2.5$

In this section, we consider the case of asymmetric absorption only for the second particle for the classical chaos parameter  $K = 2.5$  and same value of  $k = L/4 = N/8$  implying that now  $p_{\max} = 5 = (2\pi) \cdot 0.7958$  corresponds to 0.7958 classical momentum cells between 0 and  $p_{\max}$ . The statistics of Poincaré recurrences for this case was studied in [42] and here the phase space is mixed with remarkable stable islands (see Husimi figures below). This leads to a power law decay of  $P(t) \propto t^{-1}$  due to resonant classical modes outside but very close to the stable islands [42]. Similarly as in [42], we choose as initial Schmidt states localized states in momentum at (quantum) values close to  $L/3$ , more precisely:  $|u_1(0)\rangle = |p_1 = 20\Delta p\rangle$ ,  $|u_2(0)\rangle = |p_1 = 21\Delta p\rangle$ ,  $|v_1(0)\rangle = |p_2 = 21\Delta p\rangle$  and  $|v_2(0)\rangle = |p_2 = 22\Delta p\rangle$  with  $\Delta p = N/128 = L/64$  being the same scaling factor used in (12)–(15). For these values of  $p_{1,2}$  the initial momentum lines have no intersections with the stable islands. Now, the entropy  $S(t)$  does not converge (for  $U = 0$ ) or not very well (for  $U = 2$ ) and we choose for all cases a maximal iteration time of  $t_{\max} = 2^{18}$ .

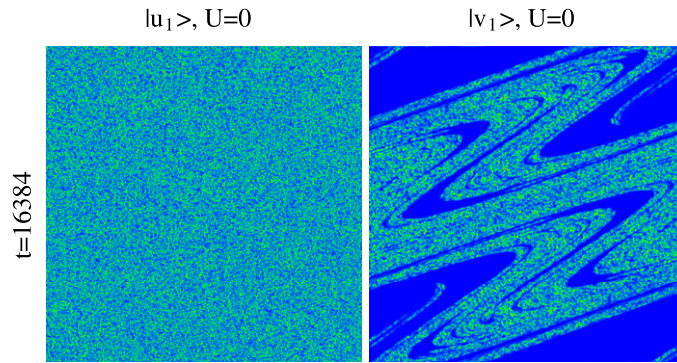


**Figure 17.** Husimi functions of the Schmidt states  $|u_1\rangle, |v_1\rangle$ , for  $U = 0, N = 65\,536$  and absorption only for the second particle at final iteration time  $t = 16\,384$ . The signification of both axes and the color codes is the same as in figure 16.

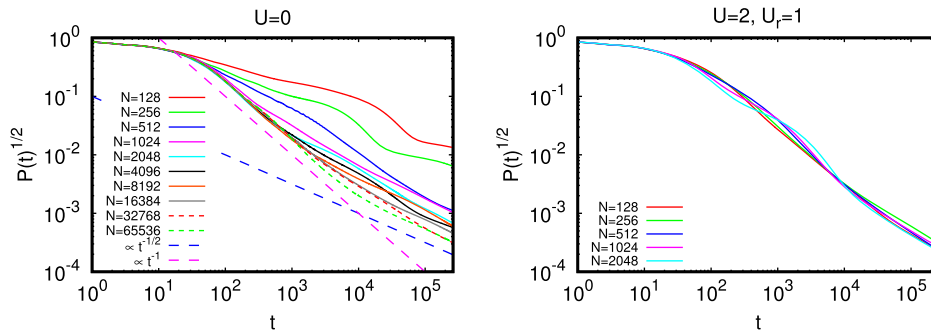


**Figure 18.** (Left) Decay of  $P(t)^{1/2} = \|\psi(t)\|$  where the norm is obtained before renormalization of the state  $|\psi(t)\rangle$  for interaction value  $U = 0$ , system size  $128 \leq N \leq 65\,536$ ,  $K = 2.5$  and absorption only for the second particle. The long dashed blue (pink) straight line corresponds to the power law  $\propto t^{-1/2}$  ( $\propto t^{-1}$ ) for comparison. (Right) Decay of  $P(t)^{1/2} = \|\psi(t)\|$  for interaction values  $U = 2, U_r = 1$  and system size  $128 \leq N \leq 2048$ . Both panels are in a double logarithmic representation.

Figure 18 shows for this case the quantity  $P(t)^{1/2}$  obtained from the quantum iteration (10) for  $U = 0$  with system size  $128 \leq N \leq 65\,536$  (left panel) and the interaction case  $U = 2, U_r = 1$  with system size  $128 \leq N \leq 2048$  (right panel). Now a double logarithmic representation is chosen since the decay is for both cases close to the power law  $P(t) \propto t^{-1}$  ( $P(t) \propto t^{-1/2}$ ) for intermediate (longer) time scales confirming the findings of [42] for  $U = 0$ . For the interaction case  $U = 2$  the decay curves for modest values of  $N$  between 128 and 2048 do not strongly depend on  $N$  (in contrast to  $U = 0$  for these size values) and are actually closer to the curves of large  $N$  values for  $U = 0$  and both types of power law decay (depending on longer or intermediate time scales).

Figure 19 shows for asymmetric absorption,  $K = 2.5, U = 0$  and different values of  $N$  the behavior of the entropy of entanglement  $S(t)$ . The entropy seems to decay for short time scales and smaller  $N$  values but has a more complicated behavior for larger time scales where the entropy may re-increase even up the initial unity value for some cases. For larger  $N$  values the initial decay is very slow and small in amplitude.

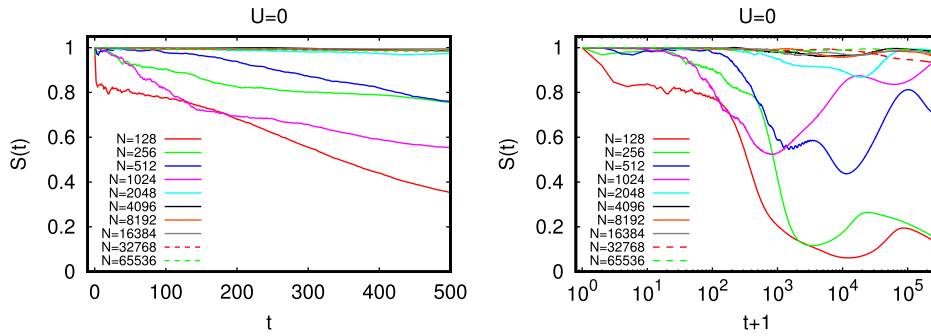


**Figure 19.** (Left) Time dependence of the entropy of entanglement  $S(t)$  for interaction value  $U = 0$ , system size  $128 \leq N \leq 65\,536$ ,  $K = 2.5$  and absorption only for the second particle. (Right) As left panel but using a logarithmic scale on the horizontal axis in  $(t + 1)$  (in order to keep the first data point at  $t = 0$  visible).

It seems that due to the weak decay of  $P(t)$  the Schmidt states  $|v_{1,2}\rangle$  of the second particle retain partly their orthogonality such that both singular values stay close to their initial values  $\alpha_1(t) \approx \alpha_2(t) \approx 1/\sqrt{2}$  implying that the entanglement is rather well conserved. However, one might expect that at extremely long exponential time scales (in  $N$ ) the entropy should also decay to 0 in a similar way the quantum decay of  $P(t)$  should become exponential for such time scales [42].

The efficient computation method for  $U = 0$  (see appendix A.1) was again used for the data of figure 19. In a similar way, as for the case  $K = 7$  (with absorption only for the second particle), the state  $|u_1(t)\rangle$  at arbitrary time  $t$  is a linear combination of both initial states  $|u_{1,2}(t=0)\rangle$  to which the free one-particle kicked rotator time evolution is applied but the coefficients of this linear combination depend on the way the second particle is absorbed. The same holds for  $|v_{1,2}(t)\rangle$  which are also given by a linear combination of both initial states  $|v_{1,2}(t=0)\rangle$  to which the free one-particle kicked rotator *with* absorption is applied. However, while for  $K = 7$  both vectors converged quite well to the first two modes of the non-unitary (one-particle) iteration operator, this is not the case for  $K = 2.5$  due to the exponentially long time scale for this type of convergence.

Figure 20 shows for the asymmetric absorption case and  $K = 2.5$  the behavior of the entropy  $S(t)$  for  $U = 2$ ,  $U_r = 1$  and system size  $128 \leq N \leq 2048$ . Initially, the entropy increases to maximum values between  $S_{\max} \approx 5$  at  $t \approx 10^2$  (for  $N = 128$ ) and  $S_{\max} \approx 7.2$  at  $t \approx 10^3$  (for  $N = 2048$ ). Interestingly, now the intermediate (first) maximum values of  $S(t)$  are larger for larger values of  $N$  (instead of smaller values of  $N$  as for  $K = 7$ ). For  $t \rightarrow \infty$  the entropy decays exponentially to a limit value  $S_\infty$  which is now significantly larger than unity (except for  $N = 128$ ) but the decay times are very long of the order of  $t_S \sim 10^5$  or even  $t_S \sim 10^6$  for  $N = 128$  and the limit value is obtained by an exponential fit with a constant term for the time interval  $2^{17} \leq t \leq 2^{18}$  ( $2^{20} \leq t \leq 2^{22}$  for  $N = 128$ ). We note that for  $N = 128$  the entropy has a minimum at  $t \approx 10^5$  and a second maximum at  $t \approx 10^6 \approx 2^{20}$  and some slight oscillatory behavior around the fit line is visible. Due to the late onset of the decay of  $S(t)$  for  $N = 128$ , we have increased the maximal iteration time here to  $t_{\max} = 2^{22}$  and in the (right panel) of figure 20 the time axis for  $N = 128$  is rescaled by a factor of  $1/16$ .

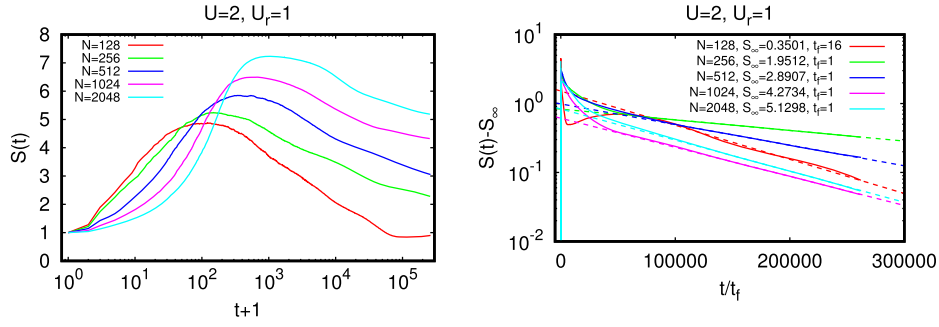


**Figure 20.** (Left) Entropy of entanglement  $S(t)$  versus iteration time for interaction values  $U = 2$ ,  $U_r = 1$ , system size  $128 \leq N \leq 2048$ ,  $K = 2.5$  and absorption only for the second particle. The horizontal axis is shown in logarithmic scale for  $(t + 1)$  (in order to keep the first data point at  $t = 0$  visible). (Right) Decay of the difference  $S(t) - S_\infty$  for the same values of interaction and system size where  $S_\infty$  is determined from the exponential fit with a constant term  $S(t) = S_\infty + S_A \exp(-t/t_S)$  for the time interval  $2^{17} \leq t \leq 2^{18}$  ( $2^{20} \leq t \leq 2^{22}$ ) for  $N \geq 256$  ( $N = 128$ ). The resulting fit values are:  $S_\infty = 0.3501 \pm 0.0039$ ,  $S_A = 1.515 \pm 0.010$ ,  $t_S = (1.403 \pm 0.017) \times 10^6$  for  $N = 128$ ;  $S_\infty = 1.9512 \pm 0.0009$ ,  $S_A = 0.8298 \pm 0.0006$ ,  $t_S = (2.808 \pm 0.006) \times 10^5$  for  $N = 256$ ;  $S_\infty = 2.8907 \pm 0.0026$ ,  $S_A = 0.9865 \pm 0.0029$ ,  $t_S = (1.452 \pm 0.014) \times 10^5$  for  $N = 512$ ;  $S_\infty = 4.2734 \pm 0.0004$ ,  $S_A = 0.6117 \pm 0.0018$ ,  $t_S = (1.030 \pm 0.004) \times 10^5$  for  $N = 1024$ ;  $S_\infty = 5.1298 \pm 0.0004$ ,  $S_A = 0.8328 \pm 0.0025$ ,  $t_S = (9.63 \pm 0.03) \times 10^4$  for  $N = 2048$ . The straight dashed lines of same color show for each value of  $N$  the resulting fit curve. The inverse scaling factor  $t_f$  on the horizontal time axis is 1 (16) for  $N \geq 256$  ( $N = 128$ ) corresponding to a maximal iteration time  $t_{\max} = 2^{18}$  ( $t_{\max} = 2^{22}$ ). The shown time scale is linear and a logarithmic scale for the vertical axis is used.

In principle, due to the obtained behavior at  $N = 128$ , we cannot exclude for certain that also for  $N \geq 256$  the entropy might re-increase at some long time with a second maximum. However, the exponential fits shown in the figure are of good quality and for all time values  $t > 10^2$  the values of  $S(t)$  are clearly above the given value of  $S_\infty$ .

For the case of this section we present additional results for the spectrum of singular values  $\alpha_i$ , and Husimi functions in figures S2–S4 of SupMat.

## 7. Discussion

In this work we studied the properties of entanglement of two particles using such tools of quantum chaos as Loschmidt echo and Poincaré recurrences with absorption.

We find that the Loschmidt echo of entanglement  $G(t_r) = \alpha t_r$  is characterized by a linear growth at small times  $t_r$  with the rate  $\alpha$  being proportional to the square of the perturbation as for the Fermi golden rule ( $\alpha \propto (\Delta U)^2$ ). We attribute such a dependence to the perturbation corrections to the Kolmogorov–Sinai entropy which is at the origin of exponentially fast wave packet spreading.

For the case of Poincaré recurrences of entanglement, we find different unusual regimes for the decay of the entropy of entanglement  $S(t)$ . For the case of absorption of both particles and in absence of interactions  $S$  always decays to zero. However this decay is very slow and depends on the system size in a complex manner. Furthermore, it is related to the gap between the first two decay rates obtained from the first two complex eigenvalues of the non-unitary one-particle iteration operator. In presence of interactions  $S$  decays to a finite value and the decay rate to it

can also be very small depending on the singular values of Schmidt decomposition. The Husimi function of the asymptotic state has a fractal repeller structure for both particles. Furthermore, the two particle state converges to an anti-symmetric state with respect to particle exchange providing double degenerate singular values appearing in the Schmidt decomposition. The entropy  $S_\infty$  of this limit state is either significantly larger than or equal to unity depending on the interaction range  $U_r = 1$  or  $U_r = 0$  respectively.

For the case of absorption of only one particle the interactions significantly modify the asymptotic Husimi function of the particle without absorption, e.g., effective repulsion structure from the other absorbed particle or faster penetration inside stable islands. The entropy of entanglement of two interacting particles also decays to a finite value. Depending on the chaos parameter the limit entropy  $S_\infty$  may be significantly below unity ( $K = 7$ ) or quite large up to  $S \approx 4-5$  ( $K = 2.5$  and largest system sizes). For the case  $K = 2.5$  the classical phase space has a hierarchical structure of integrable islands and here the time scale for the exponential entropy decay is enormously large.

Our studies are done for the case of the quantum Chirikov standard map which describes a generic behavior in the regime of quantum chaos. Indeed, other systems, as e.g. the kicked top, actively studied by Haake and his colleagues (see e.g. [62] and references therein), can be locally described by the Chirikov standard map [63]. Due to this reason we expect that the obtained results are generic.

## Acknowledgments

We enjoyed multiple friendly and chaotic discussions with Fritz Haake starting for an international workshop on quantum optics in Ustron, Poland in the fall of 1985 at the rise of perestroika.

This research was supported in part through the grant NANOX No. ANR-17-EURE-0009, (Project MTDINA) in the frame of the Programme des Investissements d’Avenir, France; the work is also supported in part by the ANR FRANCE OCTAVES (ANR-21-CE47-0007). This work was granted access to the HPC resources of CALMIP (Toulouse) under the allocation 2021-P0110.

## Data availability statement

All data that support the findings of this study are included within the article (and any supplementary files).

## Appendix A. Schmidt decomposition and singular value decomposition

### A.1. General case

The singular values  $\alpha_i(t)$  and Schmidt vectors  $|u_i(t)\rangle$  and  $|v_i(t)\rangle$  in (17) can be computed from the singular value decomposition of the ‘matrix’  $\psi(p_1, p_2)$  with  $p_1, p_2$  being the matrix indices. For this we introduce the density matrix of the first (second) particle  $\rho_1(p_1, q_1) = \sum_{p_2} \psi(p_1, p_2) \psi^*(q_1, p_2)$  (or  $\rho_2(p_2, q_2) = \sum_{p_1} \psi^*(p_1, p_2) \psi(p_1, q_2)$ ) where the  $p_2$ - ( $p_1$ -) sum corresponds to the partial trace over the second (first) particle.

In matrix notation, we can also write  $\rho_1 = \psi \psi^\dagger$  (or  $\rho_2 = \psi^\dagger \psi$ ). Note that for the asymmetric case when only one particle is absorbed the matrix  $\psi$  may be rectangular and in this case  $\rho_1$  and  $\rho_2$  may be of different size. Both matrices  $\rho_1$  and  $\rho_2$  are Hermitian and have real eigenvalues.

Let  $u_i$  be a normalized eigenvector of  $\rho_1$  with such an eigenvalue  $\lambda_i$ . Since

$$\lambda_i = \langle u_i | \rho_1 u_i \rangle = \langle u_i | \psi \psi^\dagger u_i \rangle = \langle \psi^\dagger u_i | \psi^\dagger u_i \rangle = \|\psi^\dagger u_i\|^2 \geq 0 \quad (\text{A1})$$

we write  $\lambda_i = \alpha_i^2$  with real  $\alpha_i \geq 0$ . For  $\alpha_i > 0$  let us define the (normalized) vector  $v_i = \psi^\dagger u_i / \alpha_i$  such that:

$$\rho_2 v_i = (\psi^\dagger \psi) \psi^\dagger u_i / \alpha_i = \psi^\dagger (\psi \psi^\dagger) u_i / \alpha_i = \psi^\dagger (\alpha_i^2) u_i / \alpha_i = \alpha_i^2 v_i \quad (\text{A2})$$

showing that  $v_i$  is an eigenvector of  $\rho_2$  with the same eigenvalue  $\alpha_i$ . Inversely, for a given eigenvector  $v_i$  of  $\rho_2$  with eigenvalue  $\alpha_i^2 > 0$  one can obtain by  $\tilde{u}_i = \psi v_i / \alpha_i$  a normalized eigenvector of  $\rho_1$  (which may be different from  $u_i$  for the case of a degenerate eigenvalue). Therefore,  $\rho_1$  and  $\rho_2$  have the same non-vanishing eigenvalues. Both of them may also have the eigenvalue zero but for the case of different matrix sizes it is possible that only one of them has the eigenvalue zero while the other does not. Using the eigenvectors  $u_i$  and  $v_i$ , we construct unitary matrices  $u$  and  $v$  containing these vectors in their columns respectively. (For the case of some  $\alpha_i = 0$ , we add additional column vectors orthogonal to the eigenvectors for  $\alpha_i > 0$  to obtain full squared unitary matrices.) This provides the ‘singular value decomposition’  $\psi = u \alpha v^\dagger$  where  $\alpha$  is a matrix with diagonal elements  $\alpha_i$  and zero non-diagonal elements (this matrix may be rectangular of the same size as  $\psi$ ).

This scheme provides also a numerical procedure to compute the singular value decomposition, by first diagonalizing  $\rho_1$  which gives the unitary matrix  $u$  with columns vectors  $u_i$  being the eigenvectors of  $\rho_1$ . The singular values  $\alpha_i$  are obtained as the norm  $\alpha_i = \|\psi^\dagger u_i\|$  (which is numerically more precise for small  $\alpha_i$  than taking  $\alpha_i = \sqrt{\lambda_i}$  if  $\lambda_i$  is the numerically obtained eigenvalue of  $\rho_1$ ). The eigenvectors  $v_i$  of  $\rho_2$  are then constructed as above from  $u_i$ , with eventually adding further orthogonal vectors for the case  $\alpha_i = 0$ . Once the singular value decomposition is known one chooses the columns of  $u$  for  $|u_i\rangle$  and the rows of  $v^\dagger$  (i.e. columns of  $v^*$ ) for  $|v_i\rangle$  to obtain the Schmidt decomposition (17).

For the case of a square (complex) matrix  $\psi$  (absorption of both particles) being skew-symmetric  $\psi^T = -\psi$  (e.g. the anti-symmetric state with respect to particle exchange for  $t \rightarrow \infty$  and  $U \neq 0$ ), there is a mathematical theorem [61] stating that the non-vanishing singular values come in degenerate pairs, i.e. the associated dimensions of the eigenspaces of  $\rho_{1,2}$  are even. For the simple case of a *real* skew-symmetric matrix this is quite obvious since the matrix  $\psi$  is then also anti-Hermitian ( $\psi^\dagger = -\psi$ ) with purely imaginary eigenvalues  $\pm i \alpha_j$  which also come in complex conjugated pairs (since  $\psi$  is real). The matrix relation that diagonalizes  $\psi = u D u^\dagger$  (with  $D$  being the diagonal matrix with entries  $\pm i \alpha_j$ ) becomes immediately the singular value decomposition  $\psi = u \alpha v^\dagger$  with  $v^\dagger = I u^\dagger$  where  $I$  is a diagonal matrix with entries  $\pm i$ .

However, the degeneracy for  $\alpha_i > 0$  is also valid for a *complex* skew-symmetric matrix  $\psi$  but in this case there is no simple link between the complex eigenvalues of  $\psi$  (which actually come in pairs of opposite sign) and its singular values. To get a simple understanding of this theorem (shown in [61]), we note that due to  $\psi^T = -\psi$  (now for the complex case) we have:  $\rho_2 = \psi^\dagger \psi = (-\psi)^* (-\psi^T) = (\psi \psi^\dagger)^* = \rho_1^*$ . Therefore, if  $u_i$  is an eigenvector of  $\rho_1$  we know that  $u_i^*$  is an eigenvector of  $\rho_2$  with the same eigenvalue and for  $\alpha_i > 0$  we can construct, according to the argument presented above, by  $\tilde{u}_i = \psi u_i^* / \alpha_i$  an eigenvector of  $\rho_1$ . It turns out that this new eigenvector cannot be a multiple of the initial eigenvector  $u_i$ . Assuming  $u_i = C \tilde{u}_i$ , with some phase factor  $C$ , we obtain:

$$u_i = C \psi u_i^* / \alpha_i = |C|^2 \psi \psi^* u_i / \alpha_i^2 = |C|^2 (-\psi \psi^\dagger) u_i / \alpha_i^2 = -u_i \quad (\text{A3})$$

which is impossible. Furthermore,  $\tilde{u}_i$  is even orthogonal to  $u_i$  since

$$\begin{aligned} \langle \tilde{u}_i | u_i \rangle &= \langle \psi u_i^* / \alpha_i | u_i \rangle = \langle u_i^* | \psi^\dagger u_i / \alpha_i \rangle \\ &= \langle u_i^* | -\psi^* u_i / \alpha_i \rangle = -\langle u_i^* | \tilde{u}_i^* \rangle = -\langle \tilde{u}_i | u_i \rangle \end{aligned} \tag{A4}$$

implying  $\langle \tilde{u}_i | u_i \rangle = 0$ . Therefore, for a given eigenvector  $u_i$  we can construct a second linearly independent eigenvector  $\tilde{u}_i$ . Applying the same construction scheme to  $\tilde{u}_i$  we find  $-u_i$  with a similar calculation as in (A3). Therefore the singular values different from zero are at least double degenerate and it is not difficult to argue that higher degeneracies must be even. Figure 9 provides a numerical illustration of these degeneracies for the limit state of one of the interaction cases.

### A.2. Recomputation of Schmidt decomposition for $U = 0$

In absence of interaction the quantum iteration with absorption (10) does not increase the number of Schmidt components in the initial condition, i.e., in (17) there are only two non-vanishing singular values being  $\alpha_1$  and  $\alpha_2$  and  $\alpha_i = 0$  for  $i = 3, \dots, L$ .

To see this, let us assume that we know the Schmidt decomposition (17) with  $L = 2$  components of a state  $|\psi(t)\rangle$  at a given iteration time  $t$ . In absence of interaction the iteration operator (with absorption) acts independently on the Schmidt states  $|u_{1,2}\rangle \rightarrow |\bar{u}_{1,2}\rangle$  and  $|v_{1,2}\rangle \rightarrow |\bar{v}_{1,2}\rangle$ . The new states are neither normalized neither orthogonal due to the non-unitarity of the iteration operator. However, one can normalize  $|\bar{u}_1\rangle \rightarrow |\hat{u}_1\rangle$  and  $|\bar{v}_1\rangle \rightarrow |\hat{v}_1\rangle$  and orthogonalize (by the usual Gram–Schmidt procedure)  $|\bar{u}_2\rangle$  to  $|\hat{u}_1\rangle$  and  $|\bar{v}_2\rangle$  to  $|\hat{v}_1\rangle$  resulting in new vectors  $|\hat{u}_2\rangle$  and  $|\hat{v}_2\rangle$  respectively. This procedure provides the QR-decomposition:

$$(|\bar{u}_1\rangle, |\bar{u}_2\rangle) = (|\hat{u}_1\rangle, |\hat{u}_2\rangle)R_u, \tag{A5}$$

where  $R_u$  is the upper triangular  $2 \times 2$  matrix:

$$R_u = \begin{pmatrix} \|\bar{u}_1\| & \langle \hat{u}_1 | \bar{u}_2 \rangle \\ 0 & \|\bar{u}_2\| - \langle \hat{u}_1 | \bar{u}_2 \rangle \|\hat{u}_1\| \end{pmatrix}. \tag{A6}$$

For  $|\bar{v}_{1,2}\rangle$  and  $|\hat{v}_{1,2}\rangle$  a similar relation holds using an upper triangular matrix  $R_v$ . Then the state  $|\psi(t+1)\rangle$  after one iteration can be formally written as:

$$|\psi(t+1)\rangle = (|\hat{u}_1\rangle, |\hat{u}_2\rangle)R_u \hat{\alpha}(t) R_v^T \begin{pmatrix} |\hat{v}_1\rangle^T \\ |\hat{v}_1\rangle^T \end{pmatrix}, \tag{A7}$$

where  $\hat{\alpha}(t)$  is a  $2 \times 2$  diagonal matrix with entries  $\alpha_1(t)$  and  $\alpha_2(t)$  and where the notation  $|\hat{v}_{1,2}\rangle^T$  indicates row vectors (due to the tensor product). This expression does not yet provide the Schmidt decomposition of  $|\psi(t+1)\rangle$ . For this it is necessary to compute the singular value decomposition of the  $2 \times 2$  matrix

$$A = R_u \hat{\alpha}(t) R_v^T = O_u \hat{\alpha}(t+1) O_v^T, \tag{A8}$$

where  $O_u$  and  $O_v$  are unitary  $2 \times 2$  matrices and  $\hat{\alpha}(t+1)$  is a diagonal matrix containing the new singular values  $\alpha_1(t+1)$  and  $\alpha_2(t+1)$ . The new Schmidt vectors at time  $(t+1)$  are then obtained by:

$$(|u_1(t+1)\rangle, |u_2(t+1)\rangle) = (|\hat{u}_1\rangle, |\hat{u}_2\rangle)O_u \tag{A9}$$

and similarly for  $|v_{1,2}(t+1)\rangle$  using  $O_v$ . This procedure shows that in absence of interaction the number of Schmidt components cannot increase and it provides also an efficient numerical method for the case  $U = 0$ . During the iteration the renormalization due to the absorption can be done by renormalizing the obtained new singular values (such that  $\alpha_1^2(t+1) + \alpha_2^2(t+1) = 1$ ).

Furthermore, for large times  $\alpha_2$  decays exponentially while  $\alpha_1 \rightarrow 1$  (after renormalization) but fortunately  $\alpha_2$  can be numerically computed in a very stable way, even if  $\alpha_2 \ll \alpha_1$ , using the determinant of the matrix (A8) which is  $|\det(A)| = |\det(R_u)\det(R_v)|\alpha_1(t)\alpha_2(t) = \alpha_1(t+1)\alpha_2(t+1)$ . First one computes  $\alpha_1^2(t+1)$  as the leading eigenvalue of the matrix  $A^\dagger A$  which is numerically stable and then  $\alpha_2(t+1)$  is obtained from  $\alpha_2(t+1) = |\det(A)|/\alpha_1(t+1)$ . This is also accurate for the case where the lower corner elements of the matrices  $R_u$  and  $R_v$  become very small which is possible due to the absorption process which has for long times  $t \rightarrow \infty$  the tendency to produce vectors  $|\bar{u}_{1,2}\rangle$  which are nearly parallel (and similarly for  $|\bar{v}_{1,2}\rangle$ ).

## ORCID iDs

Dima L. Shepelyansky  <https://orcid.org/0000-0002-2752-0765>

## References

- [1] Boltzmann L 1872 Weitere Studien über das Warmgleichgewicht unter Gasmolekülen *Wiener Berichte* vol 66 p 275
- [2] Loschmidt J 1876 Über den Zustand des Warmgleichgewichts eines Systems von Körpern mit Rücksicht auf die Schwerkraft *Sitzungsberichte der Akademie der Wissenschaften* vol II-73 (Wien, Austria) p 128
- [3] Boltzmann L 1877 Über die Beziehung eines Allgemeine Mechanischen Satzes zum Zweiten Hauptsatz der Warmtheorie *Sitzungsberichte der Akademie der Wissenschaften* vol II-75 (Wien, Austria) p 67
- [4] Mayer J E and Goeppert-Mayer M 1977 *Statistical Mechanics* (New York: Wiley)
- [5] Arnold V and Avez A 1968 *Ergodic Problems in Classical Mechanics* (New York: Benjamin)
- [6] Cornfeld I P, Fomin S V and Sinai Y G 1982 *Ergodic Theory* (Berlin: Springer)
- [7] Chirikov B V 1979 A universal instability of many-dimensional oscillator systems *Phys. Rep.* **52** 263
- [8] Lichtenberg A and Leiberman M 1992 *Regular and Chaotic Dynamics* (New York: Springer)
- [9] Chirikov B V, Izrailev F M and Shepelyansky D L 1981 Dynamical stochasticity in classical and quantum mechanics *Sov. Sci. Rev.* **2C** 209 [1981 Sec. C-Math. Phys. Rev., Ed. S P Novikov, 2, Harwood Acad. Publ., Chur, Switzerland]
- [10] Shepelyansky D L 1981 Dynamical stochasticity in nonlinear quantum systems *Theor. Math. Phys.* **49** 925  
Shepelyansky D L 1981 Dynamical stochasticity in nonlinear quantum systems *Teor. Mat. Fiz.* **49** 117 (in Russian)
- [11] Chirikov B V, Izrailev F M and Shepelyansky D L 1988 Quantum chaos: localization vs ergodicity *Physica D* **33** 77
- [12] Shepelyansky D 2020 Ehrenfest time and chaos *Scholarpedia* **15** 55031
- [13] Ehrenfest P 1927 Bemerkung über die angenäherte Gültigkeit der klassischen Mechanik innerhalb der Quantenmechanik *Z. Phys.* **45** 455
- [14] Gutzwiller M C 1990 *Chaos in Classical and Quantum Mechanics* (New York: Springer)
- [15] Haake F 2010 *Quantum Signatures of Chaos* (Berlin: Springer)
- [16] Shepelyansky D L 1983 Some statistical properties of simple classically stochastic quantum systems *Physica D* **8** 208
- [17] Chirikov B and Shepelyansky D 2008 Chirikov standard map *Scholarpedia* **3** 3550

- [18] Peres A 1984 Stability of quantum motion in chaotic and regular systems *Phys. Rev. A* **30** 1610
- [19] Jalabert R A and Pastawski H M 2001 Environment-independent decoherence rate in classically chaotic systems *Phys. Rev. Lett.* **86** 2490
- [20] Gorin T, Prosen T, Seligman T H and Žnidarič M 2006 Dynamics of Loschmidt echoes and fidelity decay *Phys. Rep.* **435** 33
- [21] Jacquod P and Petitjean C 2009 Decoherence, entanglement and irreversibility in quantum dynamical systems with few degrees of freedom *Adv. Phys.* **58** 67
- [22] Gousev A, Jalabert R A, Pastawski H H and Wisniacki D A 2021 Loschmidt echo *Scholarpedia* **7** 11687
- [23] Sanchez C M, Chattah A K and Pastawski H M 2021 Emergent decoherence induced by quantum chaos in a many-body system: a Loschmidt echo observation through NMR (arXiv:2112.00607)
- [24] Georgeot B and Shepelyansky D L 2001 Stable quantum computation of unstable classical chaos *Phys. Rev. Lett.* **86** 5393
- [25] Georgeot B and Shepelyansky D L 2002 Quantum computer inverting time arrow for macroscopic systems *Eur. Phys. J. D* **19** 263
- [26] Ullah A and Hoogerland M D 2011 Experimental observation of Loschmidt time reversal of a quantum chaotic system *Phys. Rev. E* **83** 046218
- [27] Martin J, Georgeot B and Shepelyansky D L 2008 Cooling by time reversal of atomic matter waves *Phys. Rev. Lett.* **100** 044106
- [28] Einstein A, Podolsky B and Rosen N 1935 Can quantum-mechanical description of physical reality be complete? *Phys. Rev.* **47** 777
- [29] Schrödinger E 1935 Die gegenwärtige situation in der quantenmechanik *Naturwissenschaften* **23** 807–12
- Schrödinger E 1935 Die gegenwärtige situation in der quantenmechanik *Naturwissenschaften* **23** 823–8
- Schrödinger E 1935 Die gegenwärtige situation in der quantenmechanik *Naturwissenschaften* **23** 844–9
- Trimmer J D 1980 The present situation in quantum mechanics: a translation of Schrödinger's 'cat paradox' paper *Proc. Am. Philos. Soc.* **124** 323 (Engl. transl.)
- [30] Nielsen M A and Chuang I L 2000 *Quantum Computation and Quantum Information* (Cambridge: Cambridge University Press)
- [31] Bengtsson I and Życzkowski K 2017 *Geometry of Quantum States: An Introduction to Quantum Entanglement* (Cambridge: Cambridge University Press)
- [32] Deutsch I H 2020 Harnessing the power of the second quantum revolution *PRX Quantum* **1** 020101
- [33] Frahm K M and Shepelyansky D L 2021 Chaotic Einstein–Podolsky–Rosen pairs, measurements and time reversal *Eur. Phys. J. D* **75** 277
- [34] Schmidt E 1907 Zur Theorie der linearen und nichtlinearen Integralgleichungen *Math. Ann.* **63** 433
- Stewart G W 2011 Fredholm, Hilbert, Schmidt: three fundamental papers on integral equations translated with commentary by G W Stewart available: <http://users.umiacs.umd.edu/~stewart/FHS.pdf> (retrieved November 2021) (Engl. transl.)
- [35] Fedorov M V and Miklin N I 2014 Schmidt modes and entanglement *Contemp. Phys.* **55** 94
- [36] Shepelyansky D L 1994 Coherent propagation of two interacting particles in a random potential *Phys. Rev. Lett.* **73** 2607
- [37] Borgonovi F and Shepelyansky D L 1995 Enhancement of localization length for two interacting kicked rotators *Nonlinearity* **8** 877
- [38] Borgonovi F, Guarneri I and Shepelyansky D L 1991 Statistics of quantum lifetimes in a classically chaotic system *Phys. Rev. A* **43** 4517
- [39] Casati G, Maspero G and Shepelyansky D L 1997 Relaxation process in a regime of quantum chaos *Phys. Rev. E* **56** R6233(R)
- [40] Savin D V and Sokolov V V 1997 Quantum versus classical decay laws in open chaotic systems *Phys. Rev. E* **56** R4911(R)
- [41] Frahm K M 1997 Quantum relaxation in open chaotic systems *Phys. Rev. E* **56** R6237(R)
- [42] Casati G, Maspero G and Shepelyansky D L 1999 Quantum Poincaré recurrences *Phys. Rev. Lett.* **82** 524
- [43] Shepelyansky D L 2008 Fractal Weyl law for quantum fractal eigenstates *Phys. Rev. E* **77** 015202(R)
- [44] Poincaré H 1890 Sur le problème des trois corps et les équations de la dynamique *Acta Math.* **13** 1–270

- [45] Chirikov B V and Shepelyansky D L 1984 *Physica D* **13** 395
- [46] Frahm K M and Shepelyansky D L 2013 Poincaré recurrences and Ulam method for the Chirikov standard map *Eur. Phys. J. B* **86** 322
- [47] Shepelyansky D L 1987 Localization of diffusive excitation in multi-level systems *Physica D* **28** 103
- [48] Fishman S, Grepel D R and Prange R E 1982 Chaos, quantum recurrences, and Anderson localization *Phys. Rev. Lett.* **49** 509
- [49] Fishman S 2010 Anderson localization and quantum chaos maps *Scholarpedia* **5** 9816
- [50] Anderson P W 1958 Absence of diffusion in certain random lattices *Phys. Rev.* **109** 1492
- [51] Moore F L, Robinson J C, Bharucha C F, Sundaram B and Raizen M G 1995 Atom optics realization of the quantum  $\delta$ -kicked rotor *Phys. Rev. Lett.* **75** 4598
- [52] Chabé J, Lemarié G, Grémaud B, Delande D, Szriftgiser P and Garreau J C 2008 Experimental observation of the Anderson metal–insulator transition with atomic matter waves *Phys. Rev. Lett.* **101** 255702
- [53] Miller P A and Sarkar S 1999 Signatures of chaos in the entanglement of two coupled quantum kicked tops *Phys. Rev. E* **60** 1542
- [54] Lakshminarayan A 2001 Entangling power of quantized chaotic systems *Phys. Rev. E* **64** 036207
- [55] Park H-K and Kim S W 2003 Decoherence from chaotic internal dynamics in two coupled  $\delta$ -function-kicked rotors *Phys. Rev. A* **67** 060102(R)
- [56] Fujisaki H, Miyadera T and Tanaka A 2003 Dynamical aspects of quantum entanglement for weakly coupled kicked tops *Phys. Rev. E* **67** 066201
- [57] Paul S and Backer A 2020 Linear and logarithmic entanglement production in an interacting chaotic system *Phys. Rev. E* **102** 050102(R)
- [58] Chirikov B V 2000 Poincaré recurrences in microtron and the global critical structure (arXiv:nlin/0006013 [nlin.CD])
- [59] Chang S-J and Shi K-J 1986 Evolution and exact eigenstates of a resonant quantum system *Phys. Rev. A* **34** 7
- [60] Frahm K M, Fleckinger R and Shepelyansky D L 2004 Quantum chaos and random matrix theory for fidelity decay in quantum computations with static imperfections *Eur. Phys. J. D* **29** 139
- [61] Horn R A and Johnson C R 2013 *Matrix Analysis* 2nd edn (Cambridge: Cambridge University Press)
- [62] Haake F and Kuś M 2010 Kicked top *Scholarpedia* **5** 10242
- [63] Haake F and Shepelyansky D L 1988 The kicked rotator as a limit of the kicked top *Europhys. Lett.* **5** 671

**Appendix S: Supplementary Material for  
“Loschmidt echo and Poincaré recurrences of entanglement”  
by L.Ermann, K.M.Frahm and D.L.Shepelyansky**

Here we present additional Figures for the main part of the article.

Additional results related to the case of absorption of two particles at the chaos parameter value  $K = 7$  (discussed in Section 4) are presented in Fig. S1.

In order to analyze the symmetry of the limit state (absorption of two particles at  $K = 7$ ) with respect to particle exchange, we decompose the state in an anti-symmetric component and a symmetric component by:

$$\psi_{\text{asym}}(p_1, p_2) = \frac{1}{2}(\psi(p_1, p_2) - \psi(p_2, p_1)) \quad (\text{S1})$$

$$\psi_{\text{sym}}(p_1, p_2) = \frac{1}{2}(\psi(p_1, p_2) + \psi(p_2, p_1)) \quad (\text{S2})$$

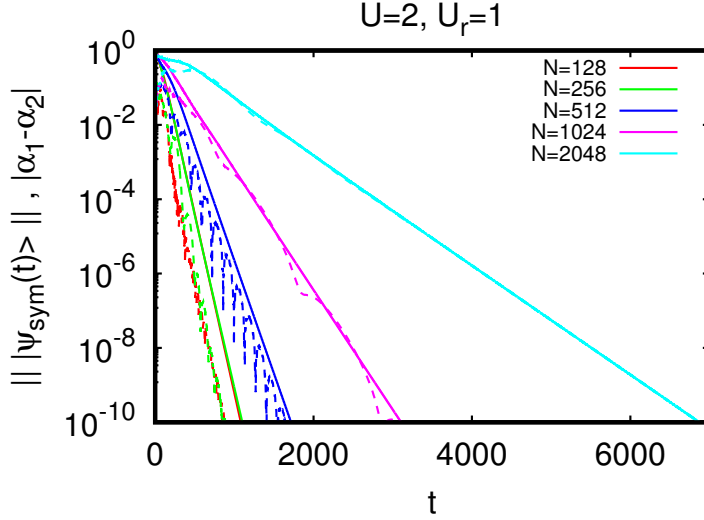
and compute the norm of both components (after renormalization of the state  $|\psi\rangle$  itself). It turns out that for all four interaction cases the symmetric component decays exponentially as can be seen in Fig. S1 (for the case  $U = 2$ ,  $U_r = 1$ ; the other cases being similar) showing the time dependence of the norm  $\|\psi_{\text{sym}}(t)\|$  and also of the difference  $|\alpha_1 - \alpha_2|$  of the first two singular values. The latter decays, apart from some oscillatory behavior, in the same way as the symmetric component showing the link between the anti-symmetry and the pairwise degeneracy of the singular values of the limit state for  $t \rightarrow \infty$ .

We mention that for  $U = 0$ , the limit state (with only one Schmidt component) is symmetric with respect to particle exchange. We have also numerically verified that this symmetry persists for very small interactions values  $U = \pm T/10$ ,  $U_r = 0, 1$  where  $T = \hbar = 56/N$  is the parameter for the free rotation part of the kicked rotator (see discussion at the beginning of section 4). Apparently, for sufficiently strong interaction (with both signs) the leading mode of the non-unitary iteration operator is anti-symmetric with respect to particle exchange which is in contrast to the behavior of vanishing or very small interaction.

Additional results for the case of absorption of only one particle at the chaos parameter value  $K = 2.5$  (discussed in Section 6) are presented in Figs. S2, S3, S4.

The large values of  $S_\infty$  (for  $K = 2.5$  and  $N \geq 256$ ) imply that many singular values contribute to the state at final iteration time  $t_{\text{max}} = 2^{18}$  as can be seen in Fig. S2. In contrast to the cases with  $K = 7$ , there is (for  $N \geq 256$ ) a considerable fraction of  $\alpha_i \gtrsim 0.1$  values (roughly for  $i \lesssim \sqrt{N/2}$ ) which contribute more uniformly to the two-particle state. Only for the case  $N = 128$  the first singular value  $\alpha_1$  is somewhat dominating.

As for the cases with  $K = 7$ , we have also computed for  $K = 2.5$  the first Schmidt vectors  $|u_{1,2}\rangle$ ,  $|v_{1,2}\rangle$  and the associated Husimi functions [59, 60, 33]. The vectors  $|u_1(t)\rangle$ ,  $|v_1(t)\rangle$  for  $U = 0$  and  $U = 2$ ,  $U_r = 1$  (all for  $N = 1024$ ) are shown in Fig. S3 for three time values being  $t = 1$ ,  $t = 8$  and  $t = t_{\text{max}} = 2^{18}$  for both  $U = 0$  and  $U = 2$ ,  $U_r = 1$ . Again for  $t = 1$ , these states occupy the same manifold but now there is no visible difference between  $U = 0$  and  $U = 2$ . Note that the available phase space for  $|v_1(t)\rangle$  is reduced by a factor of 2 concerning the maximal  $p$  value as compared to  $|u_1(t)\rangle$  and that in Fig. S3 the horizontal axis corresponds to  $\theta \in [0, 2\pi]$  in order to be coherent with the Husimi functions shown in [42] (instead of  $\theta \in [-\pi, \pi]$  in the Husimi figures for  $K = 7$ ).

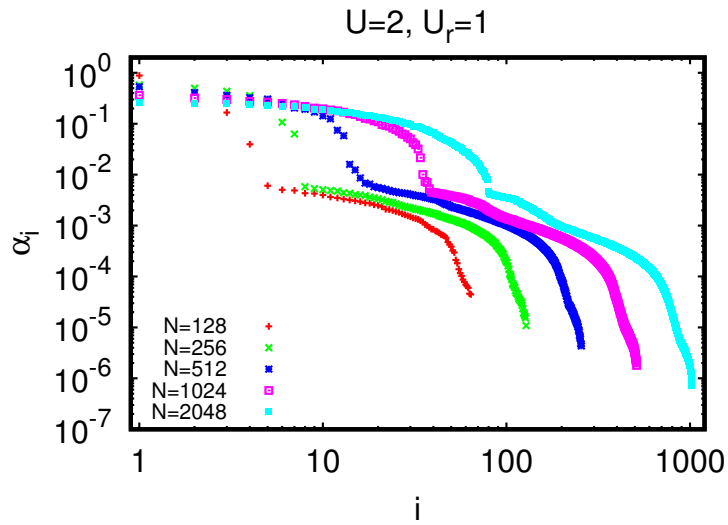


**SuppMat Figure S1.** The full lines show the decay of the norm  $\|\psi_{\text{sym}}(t)\|$  of the particle symmetrized state  $|\psi_{\text{sym}}(t)\rangle$  obtained by  $\psi_{\text{sym}}(x_1, x_2) = (\psi(x_1, x_2) + \psi(x_2, x_1))/2$  (after renormalization of  $|\psi(t)\rangle$ ) for interaction values  $U = 2, U_r = 1$  and system size  $128 \leq N \leq 2048$ . The dashed lines show for each value of  $N$  the decay of the difference  $|\alpha_1 - \alpha_2|$  where  $\alpha_{1,2}$  are the first two singular values of the state  $|\psi(t)\rangle$  becoming degenerate for  $t \rightarrow \infty$ .

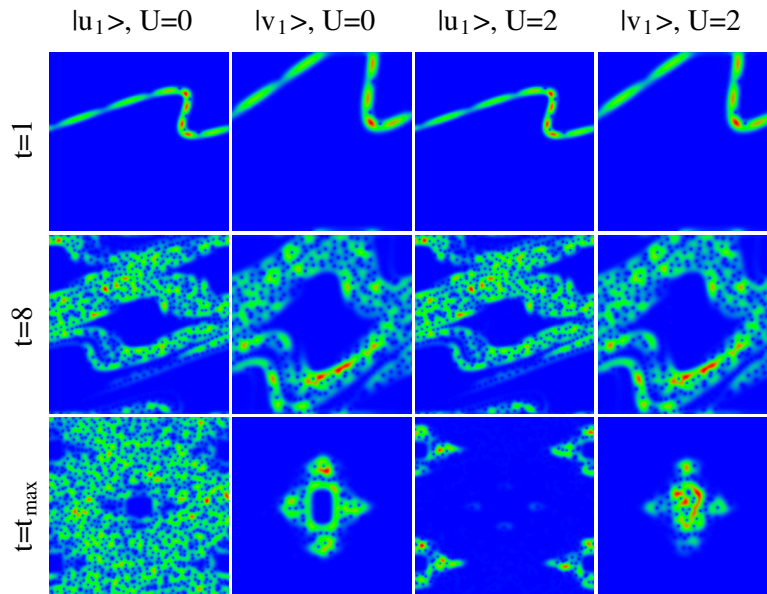
Again for  $t = 8$  the phase space structure is quite complicated but rather similar between the interacting and non-interacting cases for both states  $|u_1\rangle$  and  $|v_1\rangle$  respectively.

At long times the state  $|u_1\rangle$  of  $U = 0$  seems to be ergodic in the chaotic region of the phase space together with visible strong islands while the state  $|v_1\rangle$  of  $U = 0$  is concentrated around the stable islands but without penetrating the main center island (the other islands are quite small on the scale of the resolution of the Husimi function for  $N = 1024$ ). For  $U = 2$  the state  $|u_1\rangle$  is localized at four structures close to the corners indicating a strong repulsion of the first particle from the second particle due to the interaction. For  $U = 2$  the state  $|v_1\rangle$  is localized around the main stable island but now it penetrates inside the island quite strongly. It seems that the interaction reduces the penetration time which may be linked to the slow but well visible exponential decay of  $S(t)$  to  $S_\infty$ .

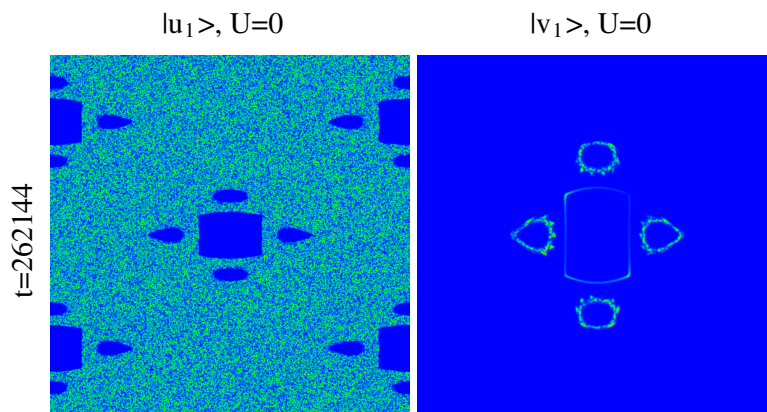
In Fig. S3, we also show for the asymmetric absorption case with  $K = 2.5$  the Husimi functions of  $|u_1\rangle$  and  $|v_1\rangle$  for  $U = 0$  and a larger system size  $N = 65536$  at final iteration time  $t = 2^{18}$ . Similarly to the case  $N = 1024$  the state  $|u_1\rangle$  is ergodic in the chaotic region of the phase space with very distinctly visible stable islands and  $|v_1\rangle$  is strongly localized around the center island (with modest density) and around the four secondary islands (with stronger density) but without penetrating these islands. The figure of  $|v_1\rangle$  is similar to the Husimi figures of Fig. 4 of [42] (which correspond to  $N = 13222$  in our notation for  $N$ ).



**SuppMat Figure S2.** Singular values  $\alpha_i$  (appearing in the Schmidt decomposition of the state  $|\psi(t = t_{\max})\rangle$  at the final iteration time  $t_{\max} = 2^{18}$ ) versus index  $i$  for interaction values  $U = 2$ ,  $U_r = 1$ , system size  $128 \leq N \leq 2048$ ,  $K = 2.5$  and absorption only for the second particle. Both axis are shown on a logarithmic scale. The values of the top singular value are  $\alpha_1 = 0.90055, 0.57604, 0.53490, 0.36280, 0.26346$  for  $N = 128, 256, 512, 1024, 2048$  respectively. (The red data point for  $N = 128$  at  $i = 2$  with  $\alpha_2 = 0.43810$  is hidden by the blue data point for  $N = 256$  with  $\alpha_2 = 0.40901$ .)



**SuppMat Figure S3.** Husimi functions of the Schmidt states  $|u_1\rangle$ ,  $|v_1\rangle$ , for  $U = 0$  or  $U = 2$  (with  $U_r = 1$ ),  $N = 1024$ ,  $K = 2.5$  and absorption only for the second particle at three iteration times  $t = 1$ ,  $t = 8$  and  $t = t_{\max} = 2^{18}$  for both  $U = 0$  and  $U = 2$ . The horizontal axis corresponds to the phase  $\theta \in [0, 2\pi]$  (different representation from former Husimi figures) and the vertical axis to the momentum  $p_{cl} \in [-2p_{\max}, 2p_{\max}]$  (for  $|u_1\rangle$ ) or  $p_{cl} \in [-p_{\max}, p_{\max}]$  (for  $|v_1\rangle$ ) where  $p_{\max} = 5 = (2\pi) \cdot 0.7958$  is the momentum absorption border in classical units (for the second particle) and  $2p_{\max}$  is the maximal classical momentum value for the full phase space in absence of absorption (for the first particle). The colors red/green/blue correspond to maximal/medium/minimal values of the Husimi function.



**SuppMat Figure S4.** Husimi functions of the Schmidt states  $|u_1\rangle$ ,  $|v_1\rangle$ , for  $U = 0$ ,  $N = 65536$ ,  $K = 2.5$  and absorption only for the second particle at final iteration time  $t = 2^{18}$ . The signification of both axes and the color codes is the same as in Fig. S3.